HHS Public Access

Author manuscript

Circulation. Author manuscript; available in PMC 2024 June 13.

Published in final edited form as:

Circulation. 2023 June 13; 147(24): 1823–1842. doi:10.1161/CIRCULATIONAHA.122.061131.

Polycomb group protein CBX7 represses cardiomyocyte proliferation via modulation of the TARDBP/RBM38 axis

Kyu-Won Cho, PhD[1], **Mark Andrade, BS**[1], **Seongho Bae, PhD**[1], **Sangsung Kim, MS**[1], **Jin Eyun Kim, MS**[1], **Er Yearn Jang, BS**[1], **Sangho Lee, PhD**[1], **Ahsan Husain, PhD**[1], **Roy L. Sutliff, PhD**[2], **John W. Calvert, PhD**[3], **Changwon Park, PhD**[4], **Young-sup Yoon, MD, PhD**[1,5]

[1]Department of Medicine, Division of Cardiology, Emory University School of Medicine, Atlanta, GA 30322, USA

[2]Division of Pulmonary, Allergy, Critical Care and Sleep Medicine, Department of Medicine, Emory University School of Medicine, Atlanta, GA 30322, USA

[3]Division of Cardiothoracic Surgery, Department of Surgery, Carlyle Fraser Heart Center, Emory University School of Medicine, Atlanta, GA 30308, USA

[4]Department of Molecular and Cellular Physiology, Louisiana State University Health Science Center, Shreveport, LA 71103, USA

[5]Severance Biomedical Science Institute, Yonsei University College of Medicine, Seoul, Republic of Korea

Abstract

Background: Shortly after birth, cardiomyocytes (CMs) exit the cell cycle and cease proliferation. At present, regulatory mechanisms for this loss of proliferative capacity are poorly understood. Chromobox 7 (CBX7), a polycomb group (PcG) protein, regulates the cell cycle, but its role in CM proliferation is unknown.

Methods: We profiled CBX7 expression in the mouse hearts via qRT-PCR, western blotting, and immunohistochemistry. We overexpressed CBX7 in neonatal mouse CMs via adenoviral transduction. We knocked down CBX7 by using constitutive and inducible conditional knockout mice (*Tnnt2-Cre;Cbx7*$^{fl/+}$ and *Myh6-MCM;Cbx7*$^{fl/fl}$, respectively). We measured CM proliferation by immunostaining of proliferation markers such as Ki67, phospho-histone 3, and cyclin B1. To examine the role of CBX7 in cardiac regeneration, we employed neonatal cardiac apical resection and adult myocardial infarction models. We examined the mechanism of CBX7-mediated repression of CM proliferation via co-immunoprecipitation, mass spectrometry, and other molecular techniques.

Result: We explored *Cbx7* expression in the heart and found that mRNA expression abruptly increased after birth and sustained throughout adulthood. Overexpression of CBX7 via adenoviral transduction reduced proliferation of neonatal CMs and promoted their multinucleation.

Correspondence: Young-sup Yoon, MD, PhD, Division of Cardiology, Department of Medicine, Emory University School of Medicine, 101 Woodruff Circle, WMB 3309, Atlanta, GA, 30322, USA, yyoon5@emory.edu, Tel: 404-727-8176.

Disclosures

None.

Conversely, genetic inactivation of *Cbx7* increased proliferation of CMs and impeded cardiac maturation during postnatal heart growth. Genetic ablation of *Cbx7* promoted regeneration of neonatal and adult injured hearts. Mechanistically, CBX7 interacted with TAR DNA-binding protein 43 (TARDBP) and positively regulated its downstream target, RNA Binding Motif Protein 38 (RBM38), in a TARDBP-dependent manner. Importantly, overexpression of RBM38 inhibited the proliferation of CBX7-depleted neonatal CMs.

Conclusions: Our results demonstrate that CBX7 directs the cell cycle exit of CMs during the postnatal period by regulating its downstream targets TARDBP and RBM38. This is the first study to demonstrate the role of CBX7 in regulation of CM proliferation, and CBX7 could be an important target for cardiac regeneration.

Keywords

polycomb; CBX7; cardiomyocyte; proliferation; cell cycle; cardiac regeneration

Introduction

Heart disease is a primary cause of mortality and morbidity worldwide, mainly because loss of CMs during heart disease is nearly irreversible due to the limited regenerative capacity of the adult heart[1–3]. CMs in mammals exit the cell cycle and cease proliferation after birth, although a very limited degree of proliferation or renewal capacity is preserved in the post-natal period[4]. Remarkable progress has been made on the mechanisms by which CMs proliferate after injury in the model organisms that regenerate the heart[5–7]. However, it is largely unknown how mammalian CMs lose proliferative capacity after birth.

Cell proliferation is controlled by Polycomb group (PcG) proteins via two distinct mechanisms[8, 9]. First, they are present in the nuclei and epigenetically control transcription of cell cycle-regulatory genes such as *CDKN2A*[10], *cyclin A*[11], *PTEN*[12], and *c-MYC*[13]. The canonical mechanism of PcG-mediated epigenetic silencing involves coordinated actions of two major types of Polycomb repressive complex (PRC), PRC1 and PRC2[14]. PRC2, consisting of EZH1/2, SUZ12, EED, and RBBP4/7, initiates the repression process by tri-methylation of histone 3 tail (H3K27me3)[15]. PRC1, composed of RING1A/B, PCGF1-6, CBX family, PHC1-3, and SCMH1/2, is then recruited and stabilizes this silencing process via mono-ubiquitination of H2A tail (H2Aub)[16]. Finally, H2Aub serves as a binding site for PRC2, which further propagates the H3K27me3 repressive histone mark on H2Aub nucleosomes, generating a positive feedback loop[17]. Second, although relatively less studied, cytoplasmic PcG proteins were also shown to control cell proliferation. EZH2, together with EED and SUZ12, forms cytosolic PRC2 and controls receptor-mediated cell proliferation in fibroblasts and T cells via its methyltransferase activity[18].

A few PcG proteins were reported to regulate CM proliferation through epigenetic regulation of transcriptional programs. Deletion of EZH2 in cardiac progenitors at an early embryonic stage reduced CM proliferation and induced cardiac defects[19]. The mechanism was proposed that EZH2 induces H3K27 trimethylation (H3K27Me3) at the loci of cyclin-dependent kinase inhibitors such as *Ink4a/b* in fetal CMs. CM-specific deletion of *Eed1* also reduced CM proliferation, causing thinning of myocardial walls and embryonic lethality,

although the mechanism has not been elucidated[19, 20]. Studies also showed that JMJ repressed CM proliferation by epigenetically downregulating cyclin D1 and by directly interacting with retinoblastoma protein[21, 22]. These reports suggest that PcG proteins play roles in CM proliferation and cardiac development through epigenetic regulation. However, no studies showed the role of a PcG protein in controlling CM proliferation through non-epigenetic gene regulation.

CBX7 is one of the PRC1 subunits and has been suggested to regulate cell proliferation, mostly in cancer cells[23–31]. However, studies reported opposite functions of CBX7 in cellular proliferation as an oncogene or a tumor suppressor. These divergent observations on CBX7 function suggest that the role of CBX7 could be tissue-specific and context-specific[32]. CBX7 acts as a reader for H3K27me3 and mediates stabilization of heterochromatin, leading to transcriptional repression of target genes[16, 33]. However, we discovered that CBX7 exists as two different alternative splicing isoforms: 36 kDa and 22 kDa proteins ($p36^{CBX7}$ and $p22^{CBX7}$, respectively)[34]. These two CBX7 isoforms found in mammals exhibit distinct characteristics. $p36^{CBX7}$ is exclusively expressed in the nucleus of proliferating cells, whereas $p22^{CBX7}$ is induced in the cytoplasm under serum deprivation and inhibits cell proliferation when overexpressed[34]. Importantly, the role of CBX7 in CM proliferation and cardiac development has not been explored.

In this study, we found that CBX7 is mainly expressed as the $p22^{CBX7}$ cytoplasmic isoform in CMs and represses proliferation of CMs during the postnatal period. During the transition from the prenatal to the postnatal stage, *Cbx7* expression abruptly increases in the heart and sustains into and during adulthood. CBX7 overexpression reduces proliferation of neonatal CMs *in vitro,* and CM-specific inhibition of *Cbx7* in conditional knock-out mice increased CM proliferation *in vivo,* promoting regeneration of neonatal and adult hearts. Mechanistically, CBX7 interacts with TARDBP, a versatile mitosis regulator, and upregulates its downstream target, RBM38, an RNA binding protein regulating cellular proliferation. Overall, this study reveals that CBX7, a PcG protein present in the cytoplasm, can function as a molecular switch to repress proliferation of CMs during the postnatal period by regulating the TARDBP/RBM38 pathway.

Materials and Methods

The data, analytical methods, and study materials will be available to other researchers for purposes of reproducing the results or replicating the procedure that are presented in this article.

Mice, Breeding and Genotyping

Mice were used in accordance with animal protocols approved by the Emory University Institutional Animal Care and Use Committee (IACUC). *Tg(Tnnt2-Cre)5Blh/JiaoJ (Tnnt2-Cre), B6.FVB(129)-A1cfTg(Myh6-Cre/Esr1*)1Jmk/J (Myh6-MCM),* and *129S4/SvJaeSor-Gt(ROSA)26Sortm1(FLP1)Dym/J (R26-FLP1)* mice were purchased from the Jackson Laboratories. ICR CD-1 mice were purchased from the Charles River Laboratories. The $Cbx7^{tm1a(KOMP)Wtsi}$ mouse was generated by the trans-NIH Knock-Out Mouse Project (KOMP). Its sperm was obtained from the KOMP Repository and rederived via IVF

and transplantation to B6 wild type donor female mice by the Mouse Transgenic and Gene Targeting Core (TMF) at Emory University. Primers used for genotyping are listed in Supplementary table 1. Purchased or rederived mice were crossed with B6 wildtype mice. Heterozygotes for either *Tg(Tnnt2-Cre)5Blh/JiaoJ* or *Cbx7*$^{tm1a(KOMP)Wtsi}$ allele were selected from F1 progenies and outcrossed with each other to generate cardiac *Cbx7*-haplodeficient mice (*Tnnt2-Cre;Cbx7*$^{fl/+}$). *Cbx7*^{floxed} mice containing the gene trapping cassette were crossbred with *R26-FLP1* mice to remove the gene trapping cassette containing *EN2SA, β-gal, IRES, Neo,* and *SV40pA*. The progeny lacking the gene trapping cassette were crossbred with *Myh6-MCM* mice. *Myh6-MCM;Cbx7*$^{fl/+}$ mice were bred to *Cbx7*$^{fl/+}$ to produce *Myh6-MCM;Cbx7*$^{fl/fl}$. Tamoxifen solution was freshly prepared on the day of injection. Tamoxifen (Sigma, T5648) was dissolved in corn oil (100%) at a concentration of 10 mg/ml by shaking 2–3 hours at 37°C. The solution was filtered with a 0.2 μm membrane. Neonatal mice (< 7 days of age) were administered 0.2 mg of tamoxifen by a single subcutaneous injection. Adult mice (> 8 weeks of age) were administered 125 μg per g (body weight) of tamoxifen by a single intraperitoneal injection.

Apical resection of the neonatal heart was performed as described previously[35]. The murine model of myocardial infarction (MI) was performed as described previously[36].

Histological analysis and immunocytochemistry

After euthanasia, mouse heart tissues were removed, fixed in 2% paraformaldehyde (PFA) at 4°C for 16 hours, and submerged in 30% sucrose solution at 4°C for 24 hours. Frozen heart sections prepared with OCT compound (Tissue-TeK 4583) were washed with PBS, and then permeabilized/blocked with PBS containing 0.5% Triton X-100 and 2.5% BSA at room temperature for 1hr. Slides were then incubated with anti-ACTN2 (Sigma, A7811, 1:100), anti-CBX7 (Abcam, ab21873, 1:100), anti-Ki67 (Cell Marque, 275R-14, 1:100), anti-phospho-Histone H3 (Ser10) (Millipore, 06-570, 1:100), anti-cyclin B1 (Cell Signaling Technology, 12231, 1:100), anti-TDP43 (TARDBP) (R&D systems, 982022, 1:100), or anti-mTOR (Cell Signaling Technology, 2983, 1:100) at 4°C overnight. WGA staining was performed by following the manufacturer's instructions (Thermo Fisher, W32466). The slides were washed three times with PBS containing 0.1% Tween 20 and incubated with appropriate secondary antibodies at room temperature for 1-2 hours. DAPI was used for nuclear staining. For immunocytochemistry, cells were fixed in 4% PFA at room temperature for 10 minutes. Then, samples were permeabilized/blocked with PBS containing 0.1% Triton X-100 and 2.5% BSA at room temperature for 1 hour. The rest of the procedure was the same as described above for immunohistochemistry. Control secondary antibodies or IgGs were used to determine the specificity of antibodies in immunostaining. The Cy5-labeled oligonucleotide (5'- UGCUCCCCGAGUGUGUUUC-3') complementary to the *Rbm38* mRNA sequence was used to stain *Rbm38* transcript. This oligonucleotide was incubated at 4°C overnight. Propidium iodide staining was performed according to the manufacturer's instructions (Thermo Fisher, P1304MP). Masson's trichome staining was performed as described previously[36]. Samples were visualized by using a Zeiss LSM 510 Meta confocal laser scanning microscope (Carl Zeiss), BZ-X800 fluorescence microscope (Keyence), and NanoZoomer-SQ digital slide scanner (Hamamatsu).

Isolation and culture of cardiac cells

Adult mouse CMs were isolated via the conventional Langendorff method as described previously[37] and used for ICC, WB, and qRT-PCR. For neonatal CM isolation, we modified a previously reported protocol[38]. Briefly, neonatal hearts from P0 mice were minced with scissors and incubated in HBSS containing 0.0125% trypsin overnight at 4°C for pre-digestion. On the following day, the tissue fragments were further digested with the Neonatal Heart Dissociation Kit (Miltenyi Biotec, 130-098-373). After filtering with a 100 μm strainer, cells were plated and cultured in plating medium (84% DMEM high glucose, 10% horse serum, 5% FBS, 1% anti-anti) at 37 °C for 1.5 hrs, allowing the preferential attachment of fibroblasts. Adherent cells were sub-cultured and used for cardiac fibroblasts which were cultured in DMEM high glucose media containing 10% FBS. Non-adherent cells were subjected to Percoll-based separation [39] and MACS using feeder removal microbeads (Miltenyi Biotec, 130-095-531) for the further purification of neonatal CMs. Enriched neonatal CMs were plated onto collagen-coated dishes and cultured in plating medium. On the following day, the medium was changed to the culture medium (78% DMEM high glucose, 17% M-199, 4% horse serum, 1% anti-anti, 1% ITS). Growth factors including 50 ng/ml IGF1 (BioLegend, 591402) and 25 ng/ml FGF1 (BioLegend, 750902) were added to both plating and culture media. Two days after the treatment with recombinant adenoviral particles, cells were subjected to ICC.

Cell culture

Mouse embryonic fibroblasts (MEFs) were cultured in DMEM high glucose medium containing 10% FBS, 1% glutamine, and 1% non-essential amino acids (NEAA). HL-1 mouse CM cell line was cultured in Claycomb Medium, supplemented with 100 μM norepinephrine, 10% fetal bovine serum (FBS), and 4 mM L-glutamine. The siRNA negative control (siNeg) and siTARDBP were purchased from Sigma Aldrich (SIC003 and EMU-219331, respectively). We transfected siRNAs using Lipofectamine™ RNAiMAX Transfection Reagent (Thermo Fisher, 13778100), following the manufacturer's instructions. Adenoviral particles were used at ~3×10^4 IFU/ml.

Generation of recombinant adenovirus particles

Molecular cloning of *Cbx7* cDNA was previously described[34]. *Rbm38* cDNA was purchased from Genecopoeia (EX-Mm34611-M83). *Cbx7* and *Rbm38* cDNAs were subcloned into an adenoviral shuttle plasmid, pDC316 (Microbix Biosystems, Mississauga, ON, Canada). Both adenoviral genomic and shuttle plasmids were transfected into HEK-293 cells using Lipofectamine 3000 (Thermo Fisher Scientific, Waltham, MA, USA). Recombinant adenoviral particles were extracted from cell lysates and the titers of adenoviral particles were determined by counting infected colonies using an antibody-mediated detection method (Clontech, Mountain View, CA, USA, Cat# 632250).

Quantitative Real-time PCR

Total RNA from mouse CMs and hearts were isolated using a guanidinium extraction method[40] combined with an RNA extraction kit (Qiagen). Extracted RNA was reverse-transcribed using Taqman Reverse Transcription Reagents (Applied Biosystems, 4304134)

according to the manufacturer's instructions. The synthesized cDNA was subjected to qRT-PCR using specific primers and probes (see Supplementary Table 1). Quantitative assessment of RNA levels was performed using an ABI PRISM 7500 Sequence Detection System (Applied Biosystems). Relative mRNA expression was normalized to Gapdh.

Western blot

Cells were lysed with RIPA buffer supplemented with PMSF, phosphatase-inhibitor cocktail (Sigma), and protease-inhibitor cocktail on ice for 1 h and the lysates were clarified by centrifugation. Equal amounts of protein were subjected to SDS-PAGE, transferred onto a polyvinylidene fluoride (PVDF) membrane, and blocked for 1 h at room temperature in Tris-buffered saline with 0.05% Tween-20 (TBST) and 5% non-fat milk. The membrane was subsequently incubated with anti-CBX7 (Abcam, ab21873, 1:1000), anti-β-actin (Cell Signaling Technology, 4967, 1:1000), anti-ACTN2 (Sigma, A7811, 1:1000), anti-RBM38 (abcam, ab200403, 1:1000), anti-TP53 (Cell Signaling Technology, 2524, 1:1000), and anti-TDP43 (TARDBP) (R&D systems, 982022, 1:2500) at 4°C overnight. After washing with TBST, blots were incubated with the appropriate secondary antibodies for 1 h at room temperature and developed using ECL detection reagent (Thermo Fisher, 32106).

MTT assay

Neonatal (P0) cardiac fibroblasts were seeded on 96 well plates at 5×10^3 cells per well. DMEM high glucose medium supplemented with 10% FBS, 1% glutamine, and 1% non-essential amino acid (NEAA) was used for culture. Two hours after seeding, cells were treated with adenoviral particles and further incubated for three days. MTT reagent was added to the cell culture at a final concentration of 0.5 mg/ml. The plate was incubated at 37ºC for 30 min in the dark. After removal of culture medium, cells were lysed by DMSO and color was measured at 570 nm.

Immunoprecipitation, silver staining, and mass spectrometry

Cytoplasmic protein fractions were extracted from MEFs or 3-month-old adult mouse hearts using NE-PER Nuclear and Cytoplasmic Extraction Reagents (Thermo Fisher, 78835). For immunoprecipitation, protein samples were pre-cleared using Dynabeads Protein G (Thermo Fisher, 10004D, 1.5 mg). Primary antibodies, rabbit IgG (Abcam, ab37415, 3 μg) or anti-CBX7 antibody (Abcam, ab21873, 3 μg), were added to the lysates and incubated at 4°C overnight with gentle agitation. To pull down protein:antibody complexes, 1.5 mg of Dynabeads Protein G was added and incubated at 4°C for 3 hrs with gentle agitation. Bead:protein:antibody complexes were washed with ice-cold PBS 6 times and denatured at 95°C for 10 min in Laemmli sample buffer supplemented with 2.5% β-mercaptoethanol. Supernatants containing protein and antibody were used for SDS-PAGE. Silver staining was performed using the Perce Silver Stain Kit (Thermo Fisher, 24612). Gel slices were reduced, carbidomethylated, dehydrated, and digested with Trypsin Gold (Promega). Following digestion, peptides were extracted and all fractions were combined. The combined fractions were concentrated using a SpeedVac to near dryness, and then resuspended to 20 μl using 95% ddH2O/5% acetonitrile (ACN)/0.1% formic acid (FA) prior to analysis by 1D reverse phase LC-nESI-MS2.

For Mass Spectrometry (MS), peptide digests (8μL each) were injected into a 1260 Infinity nHPLC stack (Agilent) and separated using a 75 micron I.D. x 15 cm pulled tip C-18 column (Jupiter C-18 300 Å, 5 micron, Phenomenex). This system was operated in-line with a Thermo Orbitrap Velos Pro hybrid mass spectrometer, which was equipped with a nano-electrospray source (Thermo Fisher Scientific). All data were collected in collision-induced dissociation (CID) mode. The nHPLC ran with binary mobile phases that included solvent A (0.1% FA in ddH2O), and solvent B (0.1% FA in 15% ddH2O/85% ACN), programmed as follows; 10 mins at 0% solvent B (2 μL/min, load), 90 mins at 0%-40% solvent B (0.5nL/min, analyze), 15 mins at 0% solvent B (2μL/min, equilibrate). Following each parent ion scan (350-1200 m/z at 60k resolution), fragmentation data (MS2) was collected on the top most intense 15 ions. For data dependent scans, charge state screening and dynamic exclusion were enabled with a repeat count of 2, repeat duration of 30 secs, and exclusion duration of 90 secs.

For MS data conversion and searches, the XCalibur RAW files were collected in profile mode, centroided and converted to MzXML using ReAdW v.3.5.1. The mgf files were then created using MzXML2 Search (included in TPP v.3.5) for all scans. The data was searched using SEQUEST, which was set for two maximum missed cleavages, a precursor mass window of 20 ppm, trypsin digestion, variable modification C at 57.0293, and M at 15.9949. Searches were performed with a species-specific subset of the UniRef100 database.

For further data analyses, the list of peptide IDs generated based on SEQUEST search results was filtered using Scaffold (Protein Sciences, Portland Oregon). Scaffold filters and groups all peptides to generate and retain only high confidence IDs while also generating normalized spectral counts (N-SC's) across all samples for the purpose of relative quantification. The filter cut-off values were set with minimum peptide length of >5 AA's, with no MH+1 charge states, with peptide probabilities of >80% C.I., and with the number of peptides per protein ≥2. The protein probabilities were then set to a >99.0% C.I., and an FDR<1.0. Scaffold incorporates the two most common methods for statistical validation of large proteome datasets, the false discovery rate (FDR) and protein probability[41–43]. Relative quantification across experiments was then performed via spectral counting[44, 45], and when relevant, spectral count abundances were normalized between samples[46].

Echocardiography

Echocardiography was performed on adult mice (3-month-old) using the Vevo 3100™ Imaging System (VisualSonics, Inc) as previously described[47]. Ejection fraction (EF) was measured using a two-dimensional method.

Statistical analyses

Investigators were blinded to the assessment of the analyses of cell, animal, and histological experiments. Both sexes were included in the animal data. For the quantification of Ki67, pH3, and cyclin $B1^+$ CMs and cell size (WGA), the results were obtained from 5 sections of the heart from each animal. All data were presented as mean ± standard error of the mean (SEM). For statistical analysis, the standard unpaired Student's t-test and one-way ANOVA test with Tukey HSD were performed. For the correlation analysis, Pearson's correlation

coefficient was calculated. P values less than 0.05 were considered statistically significant. For the data where the sample size was small (N ≤ 4), we utilized the non-parametric Mann-Whitney test (for comparing 2 sample groups). Post-MI mice that died before 4 weeks were excluded from the data collection. Sample sizes were chosen based on our experiences in the previous works.

Results

Temporal changes of polycomb group proteins in the heart

As a first step to define the roles of PcG proteins in the regulation of postnatal CM proliferation, we examined expression patterns of 18 *PcG* genes that were reported to control the cell cycle[9] (*Cbx2, Cbx4, Cbx6, Cbx7, Cbx8, Pcgf1-6, Phc1, Ring1-2, Scmh1, Ezh2, Suz12, and Yy1*) in the mouse fetal (E17.5), neonatal (P0) and adult (5-month-old) hearts by quantitative RT-PCR (qRT-PCR). Among them, 9 genes including *Cbx7, Cbx4*, and *Pcgf1* were upregulated in the neonatal heart compared to the fetal heart (Figure 1A). When comparing the gene expression between neonatal heart and adult heart, only *Cbx7* was upregulated in the adult heart, whereas 11 genes such as *Ezh2, Pcgf2,* and *Ring2* became downregulated (Figure 1A). When comparing fetal and adult hearts, only *Cbx7* was significantly upregulated while 6 genes (*Pcgf2, Ezh2, Ring2, Pcgf3, Phc1*, and *Yy1*) were downregulated in adult hearts (Figure 1A). These results indicate that *Cbx7* is the only gene significantly upregulated during the transitions from both fetal-to-neonatal and neonatal-to-adult stages with a total increase of 15.4-fold from the fetal to the adult stages. Next, to more specifically determine whether such dynamic changes of PcG gene expression occurs in cardiomyocytes (CMs), we isolated mouse neonatal (P0) and adult (3 months) CMs and performed qRT-PCR for 18 *PcG* genes (Figure S1A–B). The results showed three patterns of gene expression: upregulated (*Cbx7, Cbx8, Cbx2, Ring1a* and *Pcgf5*), downregulated (*Cbx4, Ezh2, Pcgf2* and *Ring1b*), and unchanged (*Scmh1, Pcgf6, Yy1* and *Cbx6*). Among all, *Cbx7* demonstrated the highest fold difference (~27-fold) between adult and neonatal CMs, providing the first hint at its role in the regulation of postnatal CM proliferation.

Cbx7 expression rapidly increases after birth and remains high throughout the postnatal period

Since CBX7 belongs to the family of five CBX proteins of the PRC1 complex (CBX2, -4, -6, -7, and -8)[48], we examined mRNA expression of all these genes in the heart at multiple time points from prenatal (E10.5) to postnatal (P57) periods via qRT-PCR (Figure 1B, upper panel). *Cbx2, -6,* and *-8* expression decreased from the fetal to the juvenile periods and fluctuated up and down during adulthood. *Cbx4* expression increased until the preadolescent stage and decreased afterwards. Only *Cbx7* expression showed exponential increase during the postnatal period. *Cbx7* expression increased right after birth, peaked at day 6 (at 10-fold higher than the fetal period), and maintained at a similarly high level throughout the postnatal period. To validate our findings, using the same cardiac samples, we examined expression patterns of genes for cell cycle activators and *Myh7* (an immature isoform of cardiac myosin heavy chain), which are known to undergo significant changes from the prenatal to the postnatal periods[49, 50] (Figure 1B, lower panel). As expected, *Myh7*, cyclins, and CDKs including *Ccna2, Ccnb1, Ccnb2,* and *Cdk1,* were downregulated in the

postnatal mouse hearts. Next, we sought to determine the exact time window when *Cbx7* expression increased abruptly, using fetal (E17.5 and E19.5) and neonatal mouse hearts via qRT-PCR. The results showed that *Cbx7* expression was low until E19.5 but doubled right after birth (P0) (Figure 1C). We then examined protein expression of CBX7 in adult mouse (3-month-old) CMs. Western blotting using an anti-CBX7 antibody showed that CBX7 protein was expressed with a molecular weight of 22~25 kDa (Figure 1D), suggesting that $p22^{CBX7}$ is the major isoform present in the postmitotic heart[34]. These data indicated that CBX7 expression is abruptly increased immediately after birth and sustained in postnatal CMs.

CBX7 inhibits proliferation of CMs and cardiac fibroblasts and promotes binucleation of CMs

Given that CBX7 expression sharply increases while CMs exit the cell cycle over the first week after birth, we tested whether CBX7 overexpression is able to repress proliferation of neonatal mouse CMs. For these gain-of-function analyses, we generated adenoviral particles inducing overexpression of CBX7 (Ad-CBX7) and validated its expression in both human embryonic kidney (HEK)-293 cells and mouse embryonic fibroblasts (MEFs) by western blotting (Figure S2A and Figure 1D). We further confirmed *Cbx7* expression in neonatal CMs via qRT-PCR (254-fold increase compared to Ad-Mock control) (Figure S2B), western blotting (Figure S2C), and immunocytochemistry (ICC) (Figure S2D). To determine proliferation of neonatal CMs, we infected the cells with Ad-CBX7 or Ad-Mock viral particles in the presence of growth factors such as IGF-1 and FGF-1 and conducted ICC for Ki67 (Figure 1E and Figure S2E). CBX7 overexpression resulted in a ~3.1-fold decrease in the percentage of $Ki67^+$ CMs (Figure 1F, upper panel) and ~2.2-fold increase in the percentage of binucleated CMs (Figure 1F, lower panel) compared to the Ad-Mock groups. To examine the actual changes in the CM number by CBX7 overexpression, we treated neonatal mouse CMs with either Ad-Mock or Ad-CBX7 at Day 1 and counted the number of CMs at Day 1 and Day 4, after immunostaining for ACTN2 and DAPI. We defined the day when cells were seeded as Day 0. The number of CMs at Day 4 vs Day 1 was almost doubled in the Ad-Mock-treated group (Figure S2F–G), but did not change in the Ad-CBX7 overexpression group. These results clearly show that CBX7 represses proliferation of CMs. Since the role of CBX7 is considered context- and tissue-selective[32], we further determined whether CBX7 represses proliferation of other cardiac cells. Thus, we isolated neonatal cardiac fibroblasts, infected them with Ad-CBX7 or Ad-Mock, and performed the 3-(4,5-dimethylthiazol-2-yl)-2,5-diphenyltetrazolium bromide (MTT) assay. CBX7 overexpression reduced the optical density at 570 nm up to 60%, showing that CBX7 inhibits proliferation of cardiac fibroblasts (Figure S2H). Together, these data imply an inhibitory role of CBX7 for proliferation of both CMs and cardiac fibroblasts.

CBX7 is required for normal heart development

For CBX7 loss-of-function studies, we generated CM-specific *Cbx7* knockout mice using a Cre-loxP recombination system (Figure S3A). We first generated $Cbx7^{floxed}$ mice by targeting exon 2 of the *Cbx7* gene and then cross bred them with *Tnnt2-Cre* mice to generate $Tnnt2\text{-}Cre;Cbx7^{fl/fl}$ mice (Figure S3A–3B). During generation of the conditional knockout mice, no viable homozygotes ($Tnnt2\text{-}Cre;Cbx7^{fl/fl}$) were born. However, we observed

notable phenotypes in the haplodeficient mice (*Tnnt2-Cre;Cbx7*$^{fl/+}$) such as neonatal lethality and cardiomegaly. Thus, we used the haplodeficient mice (*Tnnt2-Cre;Cbx7*$^{fl/+}$) to explore the role of CBX7. We confirmed that *Cbx7* transcript levels were less than half in the haplodeficient mice compared to the wild-type (Figure S3C).

Approximately 20% of *Tnnt2-Cre;Cbx7*$^{fl/+}$ mice died perinatally (P0-P1) (Figure S4A**)**. The rate of mortality gradually decreased over generations, suggesting reduced penetrance. The mice which were born alive but died within P1 showed abnormal behaviors such as lethargy, inactivity, and repeated convulsions immediately after birth (Figure 2A and Supplemental Movie 1 and 2). Considering relatively low expression of *Cbx7* in the embryonic heart compared to the adult heart and a previous report of viable adult *Cbx7* knockout mice[29], perinatal lethality of cardiac *Cbx7*-haplodeficient mice was unexpected. About 80% of viable mutant mice reached adulthood, but showed reduced fertility.

At P0, the heterozygotes (*Tnnt2-Cre;Cbx7*$^{fl/+}$) exhibited cardiomegaly and increased heart weight to body weight ratio (HW/BW) by 38% compared to the WT mice (Figure 2B–C and Figure S4B) while the body weight was similar between the mutant and WT mice (Figure 2C, right). Postmortem samples were excluded because their dehydrated bodies might affect the results. H & E staining showed substantially increased thickness of ventricular walls (left ventricle (LV), right ventricle (RV), and interventricular septum (IVS)) and enlarged atrium compared to the WT (Figure 2D and E). Immunostaining for ACTN2 revealed porous and sponge-like myocardium, a hallmark of fetal heart, suggesting an incomplete compaction process in *Cbx7* haplodeficient mice during heart development (Figure 2F). The mutant hearts showed 8–12% reduced mass per area compared to the WT (Figure 2G). Together, these data clearly indicate that CBX7 plays significant roles in cardiac development.

Loss of *Cbx7* in cardiomyocytes promotes cardiomyocyte proliferation and inhibits cardiomyocyte maturation

Since we observed cardiomegaly and ventricular wall thickening in the *Cbx7*-haplodeficient mice, we examined the size of CMs by wheat germ agglutinin (WGA) and ACTN2 staining. The CMs were 2.3-fold smaller in the *Cbx7* haplodeficient mice compared to the WT (Figure S5A–B), suggesting that hyperproliferation, rather than hypertrophy, of CMs is the main cause for enlarged *Cbx7* haplodeficient heart. Thus, we assessed CM proliferation in WT and *Cbx7* haplodeficient heart at P0 using double immunostaining for ACTN2 and a proliferation marker, either Ki67 or phospho-histone H3 (pH3) (Figure S6A–D). There were significantly more double-positive cells for ACTN2 and either Ki67 or pH3 in the mutant mice compared to the WT mice (Figure 3A–B). These results demonstrated that decrease of *Cbx7* expression in CMs enhances CM proliferation during postnatal heart development.

To further examine the function of CBX7 in mitotic entry of CMs, control and mutant neonatal hearts were immunostained for cyclin B1. The mutant showed a 2.8-fold increase in the percentage of cyclin B1^{+} CMs compared to the WT (Figure 3C–D and Figure S7). Cyclin B1 is one of the key regulators for mitosis. It is upregulated during the active cell cycle progression and enters the nucleus upon its activation, initiating mitotic entry[51]. Thus, the increased level of cyclin B1 in both cytoplasm and nucleus correlates with cellular proliferation. In the heart, cyclin B1 is significantly downregulated after birth (Figure

1B)[52, 53]. Recently, a study demonstrated that cyclin B1 is critical for inducing division of CMs[52]. Thus, we further assessed subcellular localization of cyclin B1 in the WT and mutant CMs and found two different staining patterns of cyclin B1 in its localization: cytoplasm only and both nuclear and cytoplasm (Figure 3E). In both localization patterns, cyclin $B1^+$ CM populations were increased in the *Cbx7* mutant mice (Figure 3F). Together, these data indicate that CBX7 is a critical repressor of mitotic entry of CMs at the postnatal stage.

We next investigated changes in the expression of genes associated with cell cycle activation and cardiac maturation with neonatal hearts via qRT-PCR (Figure S8A–D). In the mutant hearts, cell cycle activator genes involved in the G_2/M phase, *Ccna2, Ccnb1, Ccnb2,* and *Cdk1,* were upregulated. However, genes associated with cardiac maturation such as cardiac cytoskeletal/gap junction genes (*Myl7, Myl2, Tnnt2,* and *Gja1*) and cardiac ion transporting genes (*Kcnj2, Scn5a,* and *Atp2a2*) were downregulated. As for cardiac myofibril maturation, an immature isoform, *Myh7*, was upregulated but a mature isoform, *Myh6*, was downregulated. These results suggest CBX7's roles in CM cell cycle exit and CM maturation. Taken together, mice with CM-restricted inhibition of *Cbx7* have increased CM proliferation, reduced CM size, upregulation of cell cycle activator genes, and downregulation of cardiac maturation genes in the mutant heart.

CBX7 represses proliferation of CMs in the postnatal heart

We next examined the effects of *Cbx7* knockout in the postnatal heart. We generated inducible conditional knockout (iCKO) mice (*Myh6-MCM*;$Cbx7^{fl/fl}$) by cross breeding $Cbx7^{fl/fl}$ mice with *Myh6-MCM* mice. To avoid potential side effects, we first removed the gene trapping cassette from $Cbx7^{floxed}$ mice by crossbreeding with *R26-FLP1* mice (Figure 4A and Figure S9A–C). We subcutaneously injected vehicle (Control) or tamoxifen (*Cbx7* iCKO) into the neonatal mice at P0~P2 and harvested the hearts at P7 and 3 months (mo) (Figure 4B). We validated the depletion of CBX7 protein in the mutant mice by western blotting using the protein lysates collected from 3-month-old control and *Cbx7* iCKO hearts (Figure 4C). The CBX7 protein was not completely knocked out but significantly decreased. To measure CM proliferation, P7 hearts were sectioned and immunostained for Ki67, pH3, and cyclin B1. All these markers were significantly increased in iCKO CMs (Figure 4D–J and Figure S10A). At 3 months, the HW/BW ratio was increased in a subset (20%) of iCKO mice (higher than the mean plus two standard deviations (SD) of the control) which exhibited overt cardiomegaly compared to the vehicle-treated mice (Figure 4K) (Figure S10B). Ejection fraction measured by echocardiography ranged from 40% to 70% (Figure S10C). However, there was no correlation between HW/BW and ejection fraction (Figure S10D), and CM size was not affected (Figure S10E–F). Together, these data indicate that CM-specific inhibition of *Cbx7* during the postnatal period also resulted in increased CM proliferation.

Next, we wondered whether CM-specific inhibition of *Cbx7* affects postnatal cardiac maturation such as multinucleation and t-tubule formation. To examine multinucleation, we administered tamoxifen or vehicle into *Cbx7* iCKO mice at P0, and we isolated CMs three months later (Figure S11A). Then, we stained CMs with propidium iodide for nuclei

(Figure S11B). Under the bright field and epifluorescence microscopes, we examined the proportions of mono-, bi-, and multi-nucleated CMs. Compared to the control, the proportion of mononucleated CMs increased, that of binucleated CMs was reduced, and that of multinucleated (3+) CMs was not altered in the mutant heart (Figure S11C). These data suggest that CBX7 promotes binucleation of CMs. Next, we stained the control and mutant heart for t-tubules at different stages such as P0, P7, and 3 months of age (Figure S12). We used WGA for t-tubule staining. At P0, t-tubule formation was scarcely observed in both control and mutant hearts (Figure S12A). At P7, t-tubule-like structures were weakly observed in both groups (Figure S12B). These results are consistent with other reports that well-organized t-tubules are seen after 2 weeks[54]. At 3 months, we observed that t-tubules were well organized in the control but were disorganized and discontinuous in the mutant heart (Figure S12C). These results indicate that CBX7 can play an import role in the maturation of postnatal CMs.

Genetic deletion of *Cbx7* promotes regeneration of neonatal and adult hearts

To examine the role of CBX7 in neonatal heart regeneration, we employed the cardiac apical resection model. *Porrello et al* demonstrated that hearts can fully regenerate after apical resection at one day old but not at postnatal day 7 (P7), which results in scar formation[6]. Thus, we performed the apical resection surgery at P7 after we induced *Cbx7* deletion at P0 by injecting tamoxifen (Figure 5A). We performed echocardiography and harvested hearts at P28 (3 weeks after injury). Compared to the control, LVEF was increased in the *Cbx7* iCKO heart (Figure 5B). Histological analyses demonstrated that fibrosis was prominent in the control heart but was minimal in the *Cbx7* iCKO heart (Figure 5C–D). In addition, the proportions of CMs positive for Ki67, pH3, and cyclin B1 were increased in the *Cbx7* iCKO mice compared to the control (Figure 5E–F). These results suggested that *Cbx7* deletion promotes neonatal heart regeneration.

To examine the role of CBX7 in adult CM proliferation in a steady state, *Cbx7* inducible knockout mice (8 weeks old) were treated with either tamoxifen or vehicle and hearts were harvested 16 months later (Figure S13A–B). There was no significant difference between the two groups in the heart weight to body weight ratio, left ventricular ejection fraction (LVEF), or the proportion of CMs positive for Ki67, pH3, and cyclin B1 (Figure S13C-E).

To examine the role of CBX7 in adult CM proliferation following ischemic injury, *Cbx7* inducible knockout mice (5 months old) were treated with either tamoxifen or vehicle (Figure 5G). One month later, we created myocardial infarction (MI) via permanent ligation of left artery descending (LAD) of the heart[36]. Then, we examined LVEF via echocardiography and harvested the heart at 4 weeks after the surgery for histological analyses. In the *Cbx7* iCKO mice, LVEF was increased (Figure 5H), the area of fibrotic scar was reduced (Figure 5I–J), and the proportions of CMs positive for Ki67, pH3, and cyclin B1 were increased (Figure 5K–L) compared to the control. Together, these results suggest that at the adult stage, *Cbx7* deletion has minimal effects on cardiac function under stable conditions but can induce CM proliferation and improve cardiac function upon ischemic injury.

CBX7 interacts with TARDBP and controls target genes of TARDBP

Previous studies reported that CBX7 recognizes tri-methylated histones and mediates transcriptional repression by interacting with other PcG proteins in the nucleus[33]. Our recent study newly demonstrated that the short isoform of CBX7 (22-25 kDa) exists mainly in the cytoplasm, whereas the long isoform (36 kDa) is present in the nucleus[34]. As shown in Figure 1D, the major isoform in adult mouse CMs is the short isoform. When overexpressed in neonatal mouse CMs, it was localized to the cytoplasm and reduced the number of $Ki67^{+}$ CMs (Figure 1F and Figure S2D). However, the underlying mechanism whereby the short isoform of CBX7 represses cell proliferation in the cytoplasm is unknown. To explore this mechanism, we investigated potential cytoplasmic binding partners of CBX7. Mouse CBX7 was overexpressed in MEFs via adenoviral particles (Ad-CBX7). The cytoplasmic protein fraction was immunoprecipitated with anti-CBX7 antibody and subjected to SDS-PAGE followed by silver staining. Two bands were identified, which represent candidates for CBX7 binding partners (Figure 6A) and the slices for each band underwent matrix-assisted laser desorption/ionization-time of flight (MALDI-TOF) followed by mass spectrometry (MS). Proteins identified with more than 6 exclusive spectrum counts were selected (Figure 6B). We reasoned that TAR DNA-binding protein 43 (TARDBP) was the most likely binding partner for CBX7 among the candidates listed in Figure 5B, given its highest spectrum counts and known functions in cell proliferation[55–58].

Previous studies showed that TARDBP is an RNA-binding protein which regulates mitotic signaling by directly binding to mRNAs of cell cycle-related genes[55–58]. It is involved in many RNA processing pathways such as mRNA stability, pre-mRNA splicing, mRNA transport, microRNA processing, transcriptional regulation, and translational regulation[59]. TARDBP interacts with multiple proteins such as 14–3-3, copper/zinc superoxide dismutase (SOD1), and ribosomal proteins[60, 61], but the interaction with CBX7 has been unknown. To validate the mass spectrometry result, Ad-CBX7 was transduced into MEFs, and the cytoplasmic protein fraction was isolated and immunoprecipitated with anti-CBX7 antibody followed by immunoblotting with an anti-TARDBP antibody. There were three bands at 43 kDa ($p43^{TARDBP}$), 35 kDa ($p35^{TARDBP}$), and 25 kDa ($p25^{TARDBP}$) in the input, indicating three TARDBP transcript variants[62] (Figure 6C). It has been shown that all three isoforms of TARDBP can be localized to both the cytoplasm and the nucleus[62, 63]. When precipitated with anti-CBX7 antibody, all three bands were present, indicating that CBX7 binds to all three variants of TARDBP in MEFs. To determine this interaction in the postnatal heart, we conducted similar experiments with the cytoplasmic protein fraction isolated from adult mouse hearts (3-months-old). Although all three isoforms of TARDBP were detected in the cytoplasmic fraction of adult mouse heart lysates, $p43^{TARDBP}$ expression was much stronger than other isoforms (Figure 6D). The control IgG sample showed nonspecific bands at 50 kDa, 30 kDa, and 25 kDa. Immuno-precipitation with an anti-CBX7 antibody showed an additional band at 43 kDa, suggesting that CBX7 interacts with $p43^{TARDBP}$. To further validate this interaction, we performed immunostaining of the adult mouse heart with both anti-CBX7 and anti-TARDBP antibodies. CBX7 was colocalized with TARDBP, forming cytoplasmic particles in the postnatal hearts but not in the fetal hearts (Figure S14). Similar results were observed in HEK-293 cells treated with sodium arsenite, which is known to induce cytoplasmic TARDBP aggregation (Figure S15). These results are consistent with the

previous report that p43^{TARDBP} forms particles in the cytoplasm[63]. Together, these results indicated that CBX7's major binding partner is p43^{TARDBP} in the cytoplasm of the postnatal heart, although CBX7 can bind to all the alternative splicing isoforms of TARDBP.

Given the function of TARDBP in mitosis[55–58], we next investigated whether CBX7 regulates downstream target genes of TARDBP which are associated with mitosis such as *Clip1, Hormad1, Kif2a, Myo16, Pmf1, Psmd6, Rbm38, Sirt7,* and *Stag2*[58] (Figure 6E–F). First, we conducted CBX7 gain-of-function (GOF) studies by treating neonatal mouse CMs with Ad-CBX7 particles. qRT-PCR showed that only *Rbm38* was significantly increased among selected TARDBP target genes (Figure 6E). Next, we performed CBX7 loss-of-function (LOF) studies by using hearts from neonatal WT or *Cbx7* haplodeficient (*Tnnt2-Cre;Cbx7*$^{fl/+}$) mice. qRT-PCR demonstrated downregulation of all measured genes except Hormad1 (Figure 6F). Among the TARDBP target genes we examined, only two genes, *Rbm38* and Psmd6, were upregulated by CBX7 GOF and downregulated by CBX7 LOF, suggesting that they are positively regulated by CBX7. Studies reported that *Rbm38* represses cell proliferation and its deficiency causes tumorigenesis[64]. Mechanistically, RBM38 binds to the mRNA of *Cdkn1a* and maintains the stability of *Cdkn1a* transcripts, inducing cell cycle arrest at G1 phase[65]. PSMD6 is a subunit of proteasome 26S which degrades ubiquitinated proteins, regulating a variety of cellular processes such as cell cycle progression and DNA damage repair[66]. Since the function of RBM38 is more relevant to cell proliferation, we examined its expression pattern in the mouse heart from E10.5 to P480 via qRT-PCR. We found that *Rbm38* gene expression was low during the prenatal period, increased suddenly after birth, and was maintained at a high level during the postnatal period (Figure 6G). This expression pattern was similar to that of CBX7 (Figure 1B). To determine whether CBX7-mediated upregulation of *Rbm38* is dependent on TARDBP, we used siRNA transfection for *Tardbp* knockdown and adenoviral particles for CBX7 overexpression in HL-1 CMs (Figure S16). To validate siRNA transfection, we first transfected siRNA negative control (siNeg) conjugated with the fluorescent dye Cy5 into HL-1 CMs and confirmed the signal in most HL-1 CMs (Figure S16A). We further confirmed successful delivery of siRNA by visualizing siNeg-Cy5 fluorescence in the cell using confocal microscopy (Figure S16B). To optimize *Tardbp* knockdown, we transfected HL-1 CMs with siRNA for *Tardbp* (siTardbp) at different concentrations and performed western blotting (Figure S16C). We found that the TARDBP protein level was most significantly reduced by 3 nM siTardbp. This result was reproduced by comparing the protein level with siNeg control (Figure S16D). To examine CBX7-mediated induction of RBM38 at the protein level, we treated HL-1 CMs with Ad-CBX7 at different concentrations and performed western blotting. The results demonstrated that RBM38 protein was upregulated by CBX7 overexpression in a dose-dependent manner (Figure S16E). Studies showed that RBM38 upregulates TP53[67], which is known to restrict CM proliferation[68]. However, TP53 protein levels were unchanged by CBX7-mediated induction of RBM38 (Figure S16E). Finally, to determine whether TARDBP is required for CBX7-mediated induction of RBM38, we treated HL-1 CMs with siTARDBP after overexpression of CBX7 and measured protein levels of RBM38 by western blotting. The RBM38 protein level was significantly reduced by knock-down of *Tardbp* (Figure S16F). Together, these data indicate that CBX7 upregulates RBM38 in a TARDBP-dependent fashion.

The next question we addressed was how TARDBP regulates *Rbm38* expression levels in CMs. A previous report showed that TARDBP directly binds to *Rbm38* mRNA in the brain[58]. Thus, we were wondering whether a similar mechanism occurs in CMs. We treated neonatal mouse CMs with sodium arsenite, which induces cytoplasmic aggregation of TARDBP via oxidative stress. After 30 min, we harvested cells and stained for *Rbm38* mRNA, TARDBP, and TNNT2 as a CM marker. The results showed that *Rbm38* and TARDBP were colocalized in CMs (Figure S17), suggesting that TARDBP interacts with *Rbm38* mRNA. Their interaction could affect translation of *Rbm38* mRNA. This is because TARDBP is a core component of cytoplasmic stress granules (SGs) that are specialized regulatory sites of mRNA translation[69, 70].

To further examine the role of RBM38 in CM proliferation, we generated adenoviral particles inducing overexpression of RBM38 (Ad-RBM38). Neonatal CMs isolated from *Myh6-MCM;Cbx7*$^{fl/fl}$ were treated with either Ad-Mock or Ad-RBM38 in the presence of 4-hydroxytamoxifen (4-OHT) at different concentrations and cultured without growth factors for five days. Immunostaining of the cells for Ki67 and ACTN2 demonstrated that the proportion of Ki67^{+} CMs increased 2–3-fold after treatment with 4-OHT in the Ad-Mock treated group; however, such an increase was not observed in the Ad-RBM38-overexpressing CMs (Figure 6H). Finally, overexpression of CBX7 in neonatal mouse CMs promoted gene expression of *Rbm38* and *Cdkn1a* (Figure 6I). These results indicated that RBM38 is a critical downstream regulator of CBX7 in controlling CM proliferation. Taken together, these data indicate that CBX7 represses CM proliferation via modulation of the TARDBP/RBM38 pathway (Figure S18).

Discussion

Despite extensive research efforts[71], the molecular mechanisms governing loss of proliferative capacity in CMs at the early postnatal stages are poorly understood. In this study, we identified a novel pathway regulating CM proliferation by a PcG protein, CBX7. *Cbx7* expression was dramatically increased during the perinatal period and sustained in the adult heart. Constitutive deletion of *Cbx7* in CMs led to CM proliferation, cardiomegaly, and neonatal lethality. Induced deletion of *Cbx7* in CMs at the neonatal stage resulted in enhanced CM proliferation at the preadolescent stage and cardiomegaly in adulthood. While CBX7 is known as an epigenetic regulator, we found that a cytoplasmic isoform of CBX7 interacts with cell cycle regulators TARDBP and RBM38, and thus inhibits CM proliferation.

The present study is the first to demonstrate that a PcG protein, CBX7, is a key molecule associated with the perinatal transition of CMs from the proliferative to non-proliferative state. Some signaling pathways such as HIPPO, ERBB2, and MEIS1 were shown to be induced or lost in the postnatal heart to regulate CM proliferation. However, their roles in perinatal transition of CM proliferation were not reported. In this study, we identified *Cbx7* as a unique gene that is postnatally induced right after birth and represses CM proliferation. PcG proteins are important epigenetic transcriptional regulators of the cell cycle and play a crucial role in dynamically regulating the fate of cardiac progenitors during cardiac development[72]. However, their roles in postnatal CMs were unknown. We focused

on the role of a PcG protein, CBX7, as it was the most dramatically upregulated gene during the perinatal period which also sustained in the adult heart among the *PcG* genes that we examined (Figure 1). Although it is well known that CBX7 is ubiquitously expressed in many organs including the heart[23], its temporal surge in the postnatal heart was previously unknown. The role of CBX7 in cell cycle regulation was not clearly defined. Both promoting and inhibitory roles of CBX7 in cell proliferation were reported[23–31]. Our recent study provided a clue to this dispute. We discovered that CBX7 is present as two different isoforms in mammals including p36 and p22 proteins. Each isoform plays a different role according to its context and localization[34]. We found that the p22 isoform is localized in the cytoplasm and represses cell proliferation. In addition, p22 isoform is induced by serum starvation[34], which generates high levels of reactive oxygen species (ROS), triggering oxidative stress[5, 34]. This stress-induced upregulation of CBX7 may provide a clue to understand how CBX7 is induced to inhibit CM proliferation immediately after birth, when the heart is suddenly exposed to the oxygen-rich environment and faces oxidative stress, eliciting DNA damage response and cell cycle arrest in CMs[73]. Thus, this perinatal oxidative stress is a likely inducer for upregulating CBX7 after birth. Together, cytoplasmic CBX7 appears to function as a molecular switch to turn off CM proliferation in response to perinatal stresses.

The phenotype of the mice with CM-specific inhibition of *Cbx7*, such as proliferation of CMs, cardiomegaly, and perinatal mortality, supports the essential role of CBX7 in cardiac development. Increased CM proliferation in *Cbx7*-haplodeficient heart was demonstrated by Ki67 and pH3 as well as cyclin B1, which is known to be a crucial factor for inducing CM division[52]. Studies also reported that the neonatal heart exhibited downregulation of multiple cell cycle-related proteins such as cyclin A, cyclin B, cyclin D1-3, CDK1, CDK2, CDK4, and CDK6, compared to the fetal heart[53, 74–79]. Among them, cyclin B was repressed at a narrow perinatal window between E19 and P1[80]. Our data showed that *Cbx7* was induced at this stage (Figure 1) and its targeted inhibition led to derepression of cyclin B1 (Figure 3C–F), indicating that CBX7 played an important role in the repression of cyclin B1 in CMs during the perinatal period. At the organ level, *Cbx7*-haplodeficient myocardium showed cardiomegaly, increased thickness of myocardial walls, and predominant trabecular myocardium. The latter is a hallmark of the fetal heart in which CMs are proliferative. In other words, the mutant neonatal heart resembled the normal fetal heart although the heart size was bigger. This implies that the proliferative state of the fetal heart was prolonged to the neonatal stage when *Cbx7* was inhibited. In addition, we unexpectedly observed perinatal lethality in CM-restricted *Cbx7*-haplodeficient mice. Forzati *et al* reported that *Cbx7* knockout mice were viable and reached adulthood[29]. This apparent discrepancy could be due to the different knockout strategies between the previous report and our data. Forzati *et al* deleted exons 5, 6, and the 3'UTR, whereas we deleted exon 2, which constitutes the chromodomain. It is also possible that infanticide in rodents makes it difficult to observe perinatal lethality in their study.

Genetic deletion of *Cbx7* in CMs resulted in both increased CM proliferation and myocardial non-compaction. Studies have shown that myocardial non-compaction is associated with altered CM proliferation, but this association is still controversial[81–84]. We speculate that both increased CM proliferation and myocardial non-compaction contribute

to lack of myocardial maturation, leading to heart failure and perinatal lethality. Thus, our study provides insights into the pathogenesis of Left Ventricular Non-Compaction (LVNC), a myocardial abnormality where the LV wall exhibits excessive trabeculations with deep recesses, appearing as a spongy-like structure[85]. During normal heart development, formation of the trabeculae and its subsequent compaction are the key steps for ventricular chamber development[55–58]. Reports suggest that defective trabecular compaction can cause LVNC[60, 61]. Despite recent progresses with animal models, the mechanisms as to how LVNC occurs remain largely unknown. In particular, it is controversial whether LVNC is associated with increased or reduced CM proliferation[81–84]. Our data showed that incomplete/delayed compaction of myocardium could be associated with increased CM proliferation in *Cbx7* mutant mice. These results imply that uncontrolled proliferation of CMs can contribute to impeded compaction of myocardial cells.

Our study also revealed distinct effects of *Cbx7* deletion on neonatal and adult cardiac physiology. At the neonatal stage, genetic deletion of *Cbx7* in CMs resulted in reduced cardiac function even in a non-injured state (Figure S10C). At the adult stage, *Cbx7* deletion had minimal effects on cardiac function at a stable condition (Figure S13) but upon ischemic injury, improved cardiac function (Figure 5). These divergent results might have derived from differences in CM maturation state. At the neonatal stage, *Cbx7* deletion inhibited cell cycle arrest (Figure 4), and delayed maturation processes such as multinucleation (Figure 1F and Figure S11), myocardial compaction (Figure 2F–G), changes in ion channel/transporter expression (Figure S8C), and myofibril isoform switching (Figure S8D), leading to impairment of cardiac maturation and myocardial dysfunction. At the adult stage, however, important postnatal maturation processes have been completed. However, upon injury, CMs can undergo dedifferentiation and regain a capacity for cell cycle entry[86], which can enable again the effects of CBX7. Together, these results suggest that CBX7 could be a promising therapeutic target for cardiac regeneration.

We further discovered a previously unknown mechanism of regulating CM proliferation via the CBX7-TARDBP axis. TARDBP is widely expressed in various tissues including heart, lung, liver, spleen, kidney, and brain, and binds to a wide spectrum of RNAs[59]. In addition, TARDBP controls mitotic cell cycle by interacting with mRNAs of cell cycle-related genes[55–58]. Previously identified binding partners for TARDBP include SOD1 and ribosomal proteins[60, 61]. Here, we for the first time identified CBX7 as an interacting partner for TARDBP. TARDBP exists as three alternative splicing isoforms, $p43^{TARDBP}$, $p35^{TARDBP}$ and $p25^{TARDBP62}$. Our study showed that CBX7 can interact with all three isoforms of TARDBP, but its major binding partner in the postnatal heart is $p43^{TARDBP}$. We demonstrated that TARDBP interacts with CBX7 in a human cell line (HEK-293 cells), showing that this interaction is present in human as well. We also showed that CBX7 affects gene expression of multiple target mRNAs of TARDBP, including *Rbm38*. RNA-binding proteins can induce substantial changes in gene expression by inducing conformational changes of mRNA, converting the mRNA into stable or unstable states[87]. Thus, we speculate that binding of CBX7 causes conformational changes of TARDBP and its associated mRNA, leading to increased *Rbm38* mRNA. RBM38 is also an RNA-binding protein and is known to repress cell proliferation by binding to the mRNA of *Cdkn1a* and maintaining the stability of *Cdkn1a* transcripts, inducing cell cycle arrest[65]. Accordingly, our data showed

that overexpression of RBM38 repressed proliferation of neonatal CMs. In addition, gene expression of *Rbm38* and *Cdkn1a* was upregulated by overexpression of CBX7 in neonatal CMs, indicating that *Rbm38* is a critical target of CBX7/TARDBP for CM cell cycle arrest. Furthermore, the RBM38 protein level was upregulated by CBX7 overexpression in a dose-dependent manner in HL-1 CMs. Our data support our working model where CBX7 inhibits CM proliferation by interacting with TARDBP and thereby upregulating *Rbm38/Cdkn1a* during the perinatal period.

In conclusion, we identified CBX7 as a novel repressor of CM proliferation functioning during the perinatal period. CBX7 inhibits proliferation of CMs through the TARDBP/RBM38 axis. This study provides important insights into cardiac development in the context of CM proliferation.

Supplementary Material

Refer to Web version on PubMed Central for supplementary material.

Acknowledgments

We gratefully acknowledge the Emory Microscopy in Medicine (MiM) Core and the Emory Children's Pediatric Research Center flow cytometry core. We gratefully acknowledge Dr. Ho-Wook Jun and Dr. Patrick Tj Hwang for mass spectrometry analyses.

Sources of Funding

This work was supported by grants from NHLBI (R01HL150877, R01HL156008, R01HL 157242, and R01HL119291), and grants from the Bio & Medical Technology Development Program of the National Research Foundation (NRF) funded by the Korean government (MSIP) (No.2020M3A9I4038454 and No.2020R1A2C3003784). K. C. is a recipient of American Heart Association predoctoral and postdoctoral fellowship grants (16PRE31350034 and 916760).

Non-standard Abbreviations and Acronyms

CMs	cardiomyocytes
PcG	polycomb group protein
PRC	polycomb repressive complex
E17.5	embryonic day 17.5
P0	postnatal day 0
MEFs	mouse embryonic fibroblasts
$p22^{CBX7}$	transcript isoform of CBX7 with molecular weight of 22 kDa
$p43^{TARDBP}$	transcript isoform of TARDBP with molecular weight of 43 kDa

Reference

1. Braunwald E The war against heart failure: the Lancet lecture. Lancet. 2015;385:812–24. [PubMed: 25467564]

2. Velagaleti RS, Pencina MJ, Murabito JM, Wang TJ, Parikh NI, D'Agostino RB, Levy D, Kannel WB and Vasan RS. Long-term trends in the incidence of heart failure after myocardial infarction. Circulation. 2008;118:2057–62. [PubMed: 18955667]

3. Ezekowitz JA, Kaul P, Bakal JA, Armstrong PW, Welsh RC and McAlister FA. Declining in-hospital mortality and increasing heart failure incidence in elderly patients with first myocardial infarction. J Am Coll Cardiol. 2009;53:13–20. [PubMed: 19118718]

4. Senyo SE, Steinhauser ML, Pizzimenti CL, Yang VK, Cai L, Wang M, Wu TD, Guerquin-Kern JL, Lechene CP and Lee RT. Mammalian heart renewal by pre-existing cardiomyocytes. Nature. 2013;493:433–6. [PubMed: 23222518]

5. Jopling C, Sleep E, Raya M, Marti M, Raya A and Izpisua Belmonte JC. Zebrafish heart regeneration occurs by cardiomyocyte dedifferentiation and proliferation. Nature. 2010;464:606–9. [PubMed: 20336145]

6. Porrello ER, Mahmoud AI, Simpson E, Hill JA, Richardson JA, Olson EN and Sadek HA. Transient regenerative potential of the neonatal mouse heart. Science. 2011;331:1078–80. [PubMed: 21350179]

7. Kikuchi K, Holdway JE, Werdich AA, Anderson RM, Fang Y, Egnaczyk GF, Evans T, Macrae CA, Stainier DY and Poss KD. Primary contribution to zebrafish heart regeneration by gata4(+) cardiomyocytes. Nature. 2010;464:601–5. [PubMed: 20336144]

8. Sauvageau M and Sauvageau G. Polycomb group proteins: multi-faceted regulators of somatic stem cells and cancer. Cell Stem Cell. 2010;7:299–313. [PubMed: 20804967]

9. Martinez AM and Cavalli G. The role of polycomb group proteins in cell cycle regulation during development. Cell Cycle. 2006;5:1189–97. [PubMed: 16721063]

10. Jacobs JJ, Kieboom K, Marino S, DePinho RA and van Lohuizen M. The oncogene and Polycomb-group gene bmi-1 regulates cell proliferation and senescence through the ink4a locus. Nature. 1999;397:164–8. [PubMed: 9923679]

11. Martinez AM, Colomb S, Dejardin J, Bantignies F and Cavalli G. Polycomb group-dependent Cyclin A repression in Drosophila. Genes Dev. 2006;20:501–13. [PubMed: 16481477]

12. Song LB, Li J, Liao WT, Feng Y, Yu CP, Hu LJ, Kong QL, Xu LH, Zhang X, Liu WL, Li MZ, Zhang L, Kang TB, Fu LW, Huang WL, Xia YF, Tsao SW, Li M, Band V, Band H, Shi QH, Zeng YX and Zeng MS. The polycomb group protein Bmi-1 represses the tumor suppressor PTEN and induces epithelial-mesenchymal transition in human nasopharyngeal epithelial cells. J Clin Invest. 2009;119:3626–36. [PubMed: 19884659]

13. Tetsu O, Ishihara H, Kanno R, Kamiyasu M, Inoue H, Tokuhisa T, Taniguchi M and Kanno M. mel-18 negatively regulates cell cycle progression upon B cell antigen receptor stimulation through a cascade leading to c-myc/cdc25. Immunity. 1998;9:439–48. [PubMed: 9806630]

14. Bracken AP and Helin K. Polycomb group proteins: navigators of lineage pathways led astray in cancer. Nature reviews Cancer. 2009;9:773–84. [PubMed: 19851313]

15. Kirmizis A, Bartley SM, Kuzmichev A, Margueron R, Reinberg D, Green R and Farnham PJ. Silencing of human polycomb target genes is associated with methylation of histone H3 Lys 27. Genes Dev. 2004;18:1592–605. [PubMed: 15231737]

16. Ben-Saadon R, Zaaroor D, Ziv T and Ciechanover A. The polycomb protein Ring1B generates self atypical mixed ubiquitin chains required for its in vitro histone H2A ligase activity. Molecular cell. 2006;24:701–11. [PubMed: 17157253]

17. Kalb R, Latwiel S, Baymaz HI, Jansen PW, Muller CW, Vermeulen M and Muller J. Histone H2A monoubiquitination promotes histone H3 methylation in Polycomb repression. Nature structural & molecular biology. 2014;21:569–71.

18. Su IH, Dobenecker MW, Dickinson E, Oser M, Basavaraj A, Marqueron R, Viale A, Reinberg D, Wulfing C and Tarakhovsky A. Polycomb group protein ezh2 controls actin polymerization and cell signaling. Cell. 2005;121:425–36. [PubMed: 15882624]

19. He A, Ma Q, Cao J, von Gise A, Zhou P, Xie H, Zhang B, Hsing M, Christodoulou DC, Cahan P, Daley GQ, Kong SW, Orkin SH, Seidman CE, Seidman JG and Pu WT. Polycomb repressive complex 2 regulates normal development of the mouse heart. Circ Res. 2012;110:406–15. [PubMed: 22158708]

20. Dobreva G and Braun T. When silence is broken: polycomb group proteins in heart development. Circ Res. 2012;110:372–4. [PubMed: 22302750]
21. Toyoda M, Shirato H, Nakajima K, Kojima M, Takahashi M, Kubota M, Suzuki-Migishima R, Motegi Y, Yokoyama M and Takeuchi T. jumonji downregulates cardiac cell proliferation by repressing cyclin D1 expression. Dev Cell. 2003;5:85–97. [PubMed: 12852854]
22. Jung J, Kim TG, Lyons GE, Kim HR and Lee Y. Jumonji regulates cardiomyocyte proliferation via interaction with retinoblastoma protein. J Biol Chem. 2005;280:30916–23. [PubMed: 15870077]
23. Gil J, Bernard D, Martinez D and Beach D. Polycomb CBX7 has a unifying role in cellular lifespan. Nat Cell Biol. 2004;6:67–72. [PubMed: 14647293]
24. Scott CL, Gil J, Hernando E, Teruya-Feldstein J, Narita M, Martinez D, Visakorpi T, Mu D, Cordon-Cardo C, Peters G, Beach D and Lowe SW. Role of the chromobox protein CBX7 in lymphomagenesis. Proceedings of the National Academy of Sciences of the United States of America. 2007;104:5389–94. [PubMed: 17374722]
25. Pallante P, Federico A, Berlingieri MT, Bianco M, Ferraro A, Forzati F, Iaccarino A, Russo M, Pierantoni GM, Leone V, Sacchetti S, Troncone G, Santoro M and Fusco A. Loss of the CBX7 gene expression correlates with a highly malignant phenotype in thyroid cancer. Cancer research. 2008;68:6770–8. [PubMed: 18701502]
26. Karamitopoulou E, Pallante P, Zlobec I, Tornillo L, Carafa V, Schaffner T, Borner M, Diamantis I, Esposito F, Brunner T, Zimmermann A, Federico A, Terracciano L and Fusco A. Loss of the CBX7 protein expression correlates with a more aggressive phenotype in pancreatic cancer. Eur J Cancer. 2010;46:1438–44. [PubMed: 20185297]
27. Pallante P, Terracciano L, Carafa V, Schneider S, Zlobec I, Lugli A, Bianco M, Ferraro A, Sacchetti S, Troncone G, Fusco A and Tornillo L. The loss of the CBX7 gene expression represents an adverse prognostic marker for survival of colon carcinoma patients. Eur J Cancer. 2010;46:2304–13. [PubMed: 20542683]
28. Zhang XW, Zhang L, Qin W, Yao XH, Zheng LZ, Liu X, Li J and Guo WJ. Oncogenic role of the chromobox protein CBX7 in gastric cancer. Journal of experimental & clinical cancer research : CR. 2010;29:114. [PubMed: 20723236]
29. Forzati F, Federico A, Pallante P, Abbate A, Esposito F, Malapelle U, Sepe R, Palma G, Troncone G, Scarfo M, Arra C, Fedele M and Fusco A. CBX7 is a tumor suppressor in mice and humans. J Clin Invest. 2012;122:612–23. [PubMed: 22214847]
30. Kim HY, Park JH, Won HY, Lee JY and Kong G. CBX7 inhibits breast tumorigenicity through DKK-1-mediated suppression of the Wnt/beta-catenin pathway. FASEB journal : official publication of the Federation of American Societies for Experimental Biology. 2014;1:300–13.
31. Shinjo K, Yamashita Y, Yamamoto E, Akatsuka S, Uno N, Kamiya A, Niimi K, Sakaguchi Y, Nagasaka T, Takahashi T, Shibata K, Kajiyama H, Kikkawa F and Toyokuni S. Expression of chromobox homolog 7 (CBX7) is associated with poor prognosis in ovarian clear cell adenocarcinoma via TRAIL-induced apoptotic pathway regulation. International journal of cancer Journal international du cancer. 2014;135:308–18. [PubMed: 24375438]
32. Simhadri C, Daze KD, Douglas SF, Quon TT, Dev A, Gignac MC, Peng F, Heller M, Boulanger MJ, Wulff JE and Hof F. Chromodomain antagonists that target the polycomb-group methyllysine reader protein chromobox homolog 7 (CBX7). J Med Chem. 2014;57:2874–83. [PubMed: 24625057]
33. Bernstein E, Duncan EM, Masui O, Gil J, Heard E and Allis CD. Mouse polycomb proteins bind differentially to methylated histone H3 and RNA and are enriched in facultative heterochromatin. Mol Cell Biol. 2006;26:2560–9. [PubMed: 16537902]
34. Cho KW, Andrade M, Zhang Y and Yoon YS. Mammalian CBX7 isoforms p36 and p22 exhibit differential responses to serum, varying functions for proliferation, and distinct subcellular localization. Sci Rep. 2020;10:8061. [PubMed: 32415167]
35. Mahmoud AI, Porrello ER, Kimura W, Olson EN and Sadek HA. Surgical models for cardiac regeneration in neonatal mice. Nat Protoc. 2014;9:305–11. [PubMed: 24434799]
36. Cho J, Kim S, Lee H, Rah W, Cho HC, Kim NK, Bae S, Shin DH, Lee MG, Park IH, Tanaka Y, Shin E, Yi H, Han JW, Hwang PTJ, Jun HW, Park HJ, Cho K, Lee SW, Jung JK, Levit RD, Sussman MA, Harvey RP and Yoon YS. Regeneration of infarcted mouse hearts by cardiovascular

tissue formed via the direct reprogramming of mouse fibroblasts. Nat Biomed Eng. 2021;5:880–896. [PubMed: 34426676]

37. Bell RM, Mocanu MM and Yellon DM. Retrograde heart perfusion: the Langendorff technique of isolated heart perfusion. J Mol Cell Cardiol. 2011;50:940–50. [PubMed: 21385587]
38. Ehler E, Moore-Morris T and Lange S. Isolation and Culture of Neonatal Mouse Cardiomyocytes. Jove-J Vis Exp. 2013;79:50154.
39. Xu C, Police S, Rao N and Carpenter MK. Characterization and enrichment of cardiomyocytes derived from human embryonic stem cells. Circ Res. 2002;91:501–8. [PubMed: 12242268]
40. Chomczynski P and Sacchi N. Single-step method of RNA isolation by acid guanidinium thiocyanate-phenol-chloroform extraction. Anal Biochem. 1987;162:156–9. [PubMed: 2440339]
41. Nesvizhskii AI, Keller A, Kolker E and Aebersold R. A statistical model for identifying proteins by tandem mass spectrometry. Anal Chem. 2003;75:4646–58. [PubMed: 14632076]
42. Keller A, Nesvizhskii AI, Kolker E and Aebersold R. Empirical statistical model to estimate the accuracy of peptide identifications made by MS/MS and database search. Anal Chem. 2002;74:5383–92. [PubMed: 12403597]
43. Weatherly DB, Atwood JA 3rd, Minning TA, Cavola C, Tarleton RL and Orlando R. A Heuristic method for assigning a false-discovery rate for protein identifications from Mascot database search results. Mol Cell Proteomics. 2005;4:762–72. [PubMed: 15703444]
44. Old WM, Meyer-Arendt K, Aveline-Wolf L, Pierce KG, Mendoza A, Sevinsky JR, Resing KA and Ahn NG. Comparison of label-free methods for quantifying human proteins by shotgun proteomics. Mol Cell Proteomics. 2005;4:1487–502. [PubMed: 15979981]
45. Liu H, Sadygov RG and Yates JR 3rd. A model for random sampling and estimation of relative protein abundance in shotgun proteomics. Anal Chem. 2004;76:4193–201. [PubMed: 15253663]
46. Beissbarth T, Hyde L, Smyth GK, Job C, Boon WM, Tan SS, Scott HS and Speed TP. Statistical modeling of sequencing errors in SAGE libraries. Bioinformatics. 2004;20 Suppl 1:i31–9. [PubMed: 15262778]
47. Cho HJ, Lee N, Lee JY, Choi YJ, Ii M, Wecker A, Jeong JO, Curry C, Qin G and Yoon YS. Role of host tissues for sustained humoral effects after endothelial progenitor cell transplantation into the ischemic heart. J Exp Med. 2007;204:3257–69. [PubMed: 18070934]
48. Vincenz C and Kerppola TK. Different polycomb group CBX family proteins associate with distinct regions of chromatin using nonhomologous protein sequences. Proceedings of the National Academy of Sciences of the United States of America. 2008;105:16572–7. [PubMed: 18927235]
49. Pasumarthi KB and Field LJ. Cardiomyocyte cell cycle regulation. Circ Res. 2002;90:1044–54. [PubMed: 12039793]
50. Lyons GE, Schiaffino S, Sassoon D, Barton P and Buckingham M. Developmental regulation of myosin gene expression in mouse cardiac muscle. J Cell Biol. 1990;111:2427–36. [PubMed: 2277065]
51. Jin P, Hardy S and Morgan DO. Nuclear localization of cyclin B1 controls mitotic entry after DNA damage. J Cell Biol. 1998;141:875–85. [PubMed: 9585407]
52. Mohamed TMA, Ang YS, Radzinsky E, Zhou P, Huang Y, Elfenbein A, Foley A, Magnitsky S and Srivastava D. Regulation of Cell Cycle to Stimulate Adult Cardiomyocyte Proliferation and Cardiac Regeneration. Cell. 2018;173:104–116 e12. [PubMed: 29502971]
53. Yoshizumi M, Lee WS, Hsieh CM, Tsai JC, Li J, Perrella MA, Patterson C, Endege WO, Schlegel R and Lee ME. Disappearance of cyclin A correlates with permanent withdrawal of cardiomyocytes from the cell cycle in human and rat hearts. J Clin Invest. 1995;95:2275–80. [PubMed: 7738192]
54. Hamaguchi S, Kawakami Y, Honda Y, Nemoto K, Sano A, Namekata I and Tanaka H. Developmental changes in excitation-contraction mechanisms of the mouse ventricular myocardium as revealed by functional and confocal imaging analyses. J Pharmacol Sci. 2013;123:167–75. [PubMed: 24096881]
55. De Conti L, Akinyi MV, Mendoza-Maldonado R, Romano M, Baralle M and Buratti E. TDP-43 affects splicing profiles and isoform production of genes involved in the apoptotic and mitotic cellular pathways. Nucleic Acids Res. 2015;43:8990–9005. [PubMed: 26261209]

56. Zhao L, Li L, Xu H, Ke H, Zou L, Yang Q, Shen CJ, Nie J and Jiao B. TDP-43 is Required for Mammary Gland Repopulation and Proliferation of Mammary Epithelial Cells. Stem Cells Dev. 2019;28:944–953. [PubMed: 31062657]
57. Ayala YM, Misteli T and Baralle FE. TDP-43 regulates retinoblastoma protein phosphorylation through the repression of cyclin-dependent kinase 6 expression. Proceedings of the National Academy of Sciences of the United States of America. 2008;105:3785–9. [PubMed: 18305152]
58. Tollervey JR, Curk T, Rogelj B, Briese M, Cereda M, Kayikci M, Konig J, Hortobagyi T, Nishimura AL, Zupunski V, Patani R, Chandran S, Rot G, Zupan B, Shaw CE and Ule J. Characterizing the RNA targets and position-dependent splicing regulation by TDP-43. Nat Neurosci. 2011;14:452–8. [PubMed: 21358640]
59. Buratti E and Baralle FE. TDP-43: gumming up neurons through protein-protein and protein-RNA interactions. Trends Biochem Sci. 2012;37:237–47. [PubMed: 22534659]
60. Volkening K, Leystra-Lantz C, Yang W, Jaffee H and Strong MJ. Tar DNA binding protein of 43 kDa (TDP-43), 14-3-3 proteins and copper/zinc superoxide dismutase (SOD1) interact to modulate NFL mRNA stability. Implications for altered RNA processing in amyotrophic lateral sclerosis (ALS). Brain Res. 2009;1305:168–82. [PubMed: 19815002]
61. Freibaum BD, Chitta RK, High AA and Taylor JP. Global analysis of TDP-43 interacting proteins reveals strong association with RNA splicing and translation machinery. J Proteome Res. 2010;9:1104–20. [PubMed: 20020773]
62. Nishimoto Y, Ito D, Yagi T, Nihei Y, Tsunoda Y and Suzuki N. Characterization of alternative isoforms and inclusion body of the TAR DNA-binding protein-43. J Biol Chem. 2010;285:608–19. [PubMed: 19887443]
63. Gasset-Rosa F, Lu S, Yu H, Chen C, Melamed Z, Guo L, Shorter J, Da Cruz S and Cleveland DW. Cytoplasmic TDP-43 De-mixing Independent of Stress Granules Drives Inhibition of Nuclear Import, Loss of Nuclear TDP-43, and Cell Death. Neuron. 2019;102:339–357 e7. [PubMed: 30853299]
64. Zhang J, Xu E, Ren C, Yan W, Zhang M, Chen M, Cardiff RD, Imai DM, Wisner E and Chen X. Mice deficient in Rbm38, a target of the p53 family, are susceptible to accelerated aging and spontaneous tumors. Proceedings of the National Academy of Sciences of the United States of America. 2014;111:18637–42. [PubMed: 25512531]
65. Shu L, Yan W and Chen X. RNPC1, an RNA-binding protein and a target of the p53 family, is required for maintaining the stability of the basal and stress-induced p21 transcript. Genes Dev. 2006;20:2961–72. [PubMed: 17050675]
66. Voges D, Zwickl P and Baumeister W. The 26S proteasome: a molecular machine designed for controlled proteolysis. Annu Rev Biochem. 1999;68:1015–68. [PubMed: 10872471]
67. Ye J, Liang R, Bai T, Lin Y, Mai R, Wei M, Ye X, Li L and Wu F. RBM38 plays a tumor-suppressor role via stabilizing the p53-mdm2 loop function in hepatocellular carcinoma. Journal of experimental & clinical cancer research : CR. 2018;37:212. [PubMed: 30176896]
68. Shoffner A, Cigliola V, Lee N, Ou J and Poss KD. Tp53 Suppression Promotes Cardiomyocyte Proliferation during Zebrafish Heart Regeneration. Cell Rep. 2020;32:108089. [PubMed: 32877671]
69. Mokas S, Mills JR, Garreau C, Fournier MJ, Robert F, Arya P, Kaufman RJ, Pelletier J and Mazroui R. Uncoupling stress granule assembly and translation initiation inhibition. Mol Biol Cell. 2009;20:2673–83. [PubMed: 19369421]
70. Colombrita C, Zennaro E, Fallini C, Weber M, Sommacal A, Buratti E, Silani V and Ratti A. TDP-43 is recruited to stress granules in conditions of oxidative insult. J Neurochem. 2009;111:1051–61. [PubMed: 19765185]
71. Sadek H and Olson EN. Toward the Goal of Human Heart Regeneration. Cell Stem Cell. 2020;26:7–16. [PubMed: 31901252]
72. Wang QT. Epigenetic regulation of cardiac development and function by polycomb group and trithorax group proteins. Dev Dyn. 2012;241:1021–33. [PubMed: 22514007]
73. Puente BN, Kimura W, Muralidhar SA, Moon J, Amatruda JF, Phelps KL, Grinsfelder D, Rothermel BA, Chen R, Garcia JA, Santos CX, Thet S, Mori E, Kinter MT, Rindler PM, Zacchigna S, Mukherjee S, Chen DJ, Mahmoud AI, Giacca M, Rabinovitch PS, Aroumougame

A, Shah AM, Szweda LI and Sadek HA. The oxygen-rich postnatal environment induces cardiomyocyte cell-cycle arrest through DNA damage response. Cell. 2014;157:565–79. [PubMed: 24766806]

74. Brooks G, Poolman RA, McGill CJ and Li JM. Expression and activities of cyclins and cyclin-dependent kinases in developing rat ventricular myocytes. J Mol Cell Cardiol. 1997;29:2261–71. [PubMed: 9281457]
75. Chen HW, Yu SL, Chen WJ, Yang PC, Chien CT, Chou HY, Li HN, Peck K, Huang CH, Lin FY, Chen JJ and Lee YT. Dynamic changes of gene expression profiles during postnatal development of the heart in mice. Heart. 2004;90:927–34. [PubMed: 15253972]
76. Kang MJ, Kim JS, Chae SW, Koh KN and Koh GY. Cyclins and cyclin dependent kinases during cardiac development. Mol Cells. 1997;7:360–6. [PubMed: 9264023]
77. Liao HS, Kang PM, Nagashima H, Yamasaki N, Usheva A, Ding B, Lorell BH and Izumo S. Cardiac-specific overexpression of cyclin-dependent kinase 2 increases smaller mononuclear cardiomyocytes. Circ Res. 2001;88:443–50. [PubMed: 11230113]
78. Soonpaa MH, Kim KK, Pajak L, Franklin M and Field LJ. Cardiomyocyte DNA synthesis and binucleation during murine development. Am J Physiol. 1996;271:H2183–9. [PubMed: 8945939]
79. Soonpaa MH, Koh GY, Pajak L, Jing S, Wang H, Franklin MT, Kim KK and Field LJ. Cyclin D1 overexpression promotes cardiomyocyte DNA synthesis and multinucleation in transgenic mice. J Clin Invest. 1997;99:2644–54. [PubMed: 9169494]
80. Kang MJ and Koh GY. Differential and dramatic changes of cyclin-dependent kinase activities in cardiomyocytes during the neonatal period. J Mol Cell Cardiol. 1997;29:1767–77. [PubMed: 9236132]
81. Kosaka Y, Cieslik KA, Li L, Lezin G, Maguire CT, Saijoh Y, Toyo-oka K, Gambello MJ, Vatta M, Wynshaw-Boris A, Baldini A, Yost HJ and Brunelli L. 14-3-3epsilon plays a role in cardiac ventricular compaction by regulating the cardiomyocyte cell cycle. Mol Cell Biol. 2012;32:5089–102. [PubMed: 23071090]
82. Chen Q, Chen H, Zheng D, Kuang C, Fang H, Zou B, Zhu W, Bu G, Jin T, Wang Z, Zhang X, Chen J, Field LJ, Rubart M, Shou W and Chen Y. Smad7 is required for the development and function of the heart. J Biol Chem. 2009;284:292–300. [PubMed: 18952608]
83. DiMichele LA, Hakim ZS, Sayers RL, Rojas M, Schwartz RJ, Mack CP and Taylor JM. Transient expression of FRNK reveals stage-specific requirement for focal adhesion kinase activity in cardiac growth. Circ Res. 2009;104:1201–8. [PubMed: 19372463]
84. Shou W, Aghdasi B, Armstrong DL, Guo Q, Bao S, Charng MJ, Mathews LM, Schneider MD, Hamilton SL and Matzuk MM. Cardiac defects and altered ryanodine receptor function in mice lacking FKBP12. Nature. 1998;391:489–92. [PubMed: 9461216]
85. Chin TK, Perloff JK, Williams RG, Jue K and Mohrmann R. Isolated noncompaction of left ventricular myocardium. A study of eight cases. Circulation. 1990;82:507–13. [PubMed: 2372897]
86. Wang WE, Li L, Xia X, Fu W, Liao Q, Lan C, Yang D, Chen H, Yue R, Zeng C, Zhou L, Zhou B, Duan DD, Chen X, Houser SR and Zeng C. Dedifferentiation, Proliferation, and Redifferentiation of Adult Mammalian Cardiomyocytes After Ischemic Injury. Circulation. 2017;136:834–848. [PubMed: 28642276]
87. Garneau NL, Wilusz J and Wilusz CJ. The highways and byways of mRNA decay. Nat Rev Mol Cell Biol. 2007;8:113–26. [PubMed: 17245413]

Clinical Perspective

What Is New?

- Cardiac expression of *Cbx7* gene is abruptly upregulated after birth and sustained throughout adulthood.
- Genetic ablation of *Cbx7* inhibits myocardial maturation and compaction, suggesting that *Cbx7* expression is critical for normal heart development.
- Targeted inhibition of *Cbx7* gene in cardiomyocytes (CMs) induces proliferation of CMs, promoting cardiac regeneration in mice.
- CBX7 interacts with TARDBP and positively regulates its downstream target, RBM38, in a TARDBP-dependent manner.

What Are the Clinical Implications?

- Genetic ablation of *Cbx7* induces proliferation of CMs, cardiomegaly, myocardial non-compaction, and perinatal mortality, suggesting that CBX7 can play an important role for cardiac development and genetic cardiac diseases.
- Genetic inactivation of *Cbx7* in postnatal CMs induces proliferation of CMs and promotes cardiac regeneration, supporting that CBX7 could be a promising target for cardiac regeneration after myocardial injury.

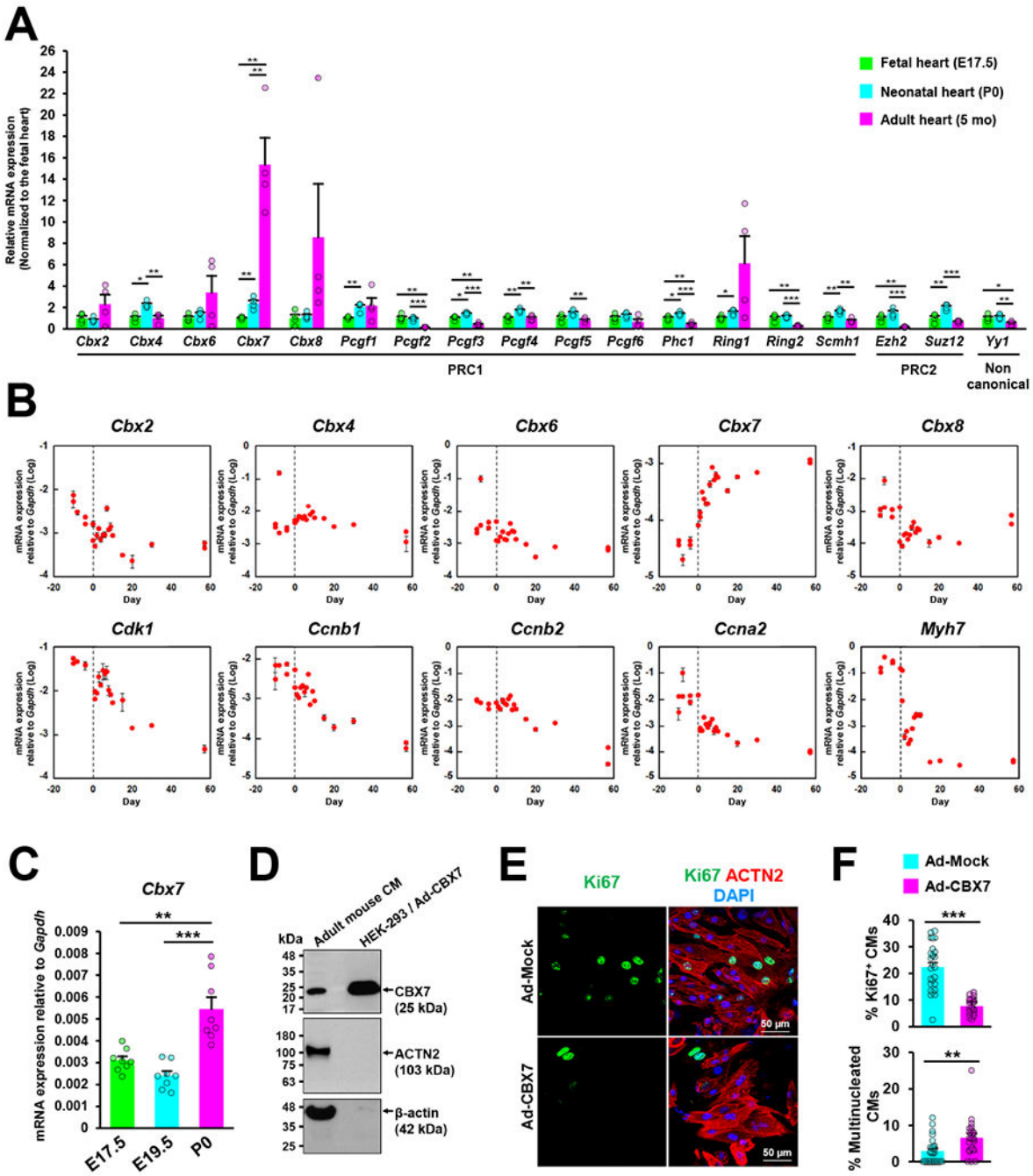

Figure 1. Expression profiling of Polycomb group genes in mouse hearts and CMs.

A. mRNA expression of *PcG* genes in the mouse heart. Expression of 18 *PcG* genes was examined in fetal (E17.5), neonatal (P0), and adult (5 months) hearts by qRT-PCR and the fold change was calculated by normalizing to the fetal heart values. *P < 0.05, **P < 0.01, ***P < 0.001. Mann-Whitney tests were performed comparing fetal vs. neonatal hearts, neonatal vs. adult hearts, and fetal vs. adult hearts. N = 4, each with technical triplicates.

B. mRNA levels of the indicated genes in the mouse hearts measured by qRT-PCR at different developmental stages from E10.5 to 60 days after birth. N = 22, each with technical

triplicates. **C.** mRNA levels of *Cbx7* in mouse hearts showing perinatal upregulation. **P < 0.01, ***P < 0.001. One-way ANOVA test with Tukey HSD. N = 8, each with technical triplicates. **D.** Western blot for CBX7 using isolated adult mouse CMs. HEK-293 cells infected with Ad-CBX7 were used as a positive control. **E.** Double immunostaining of neonatal mouse CMs transduced with Ad-CBX7 for ACTN2 and Ki67 and cultured in the presence of growth factors including IGF-1 and FGF-1 for three days. DAPI (blue). **F.** Percentages of $Ki67^{+}$ CMs and multinucleated CMs. *P < 0.05, **P < 0.01, ***P < 0.001. Standard unpaired Student's t test. More than 500 cells in each group were examined.

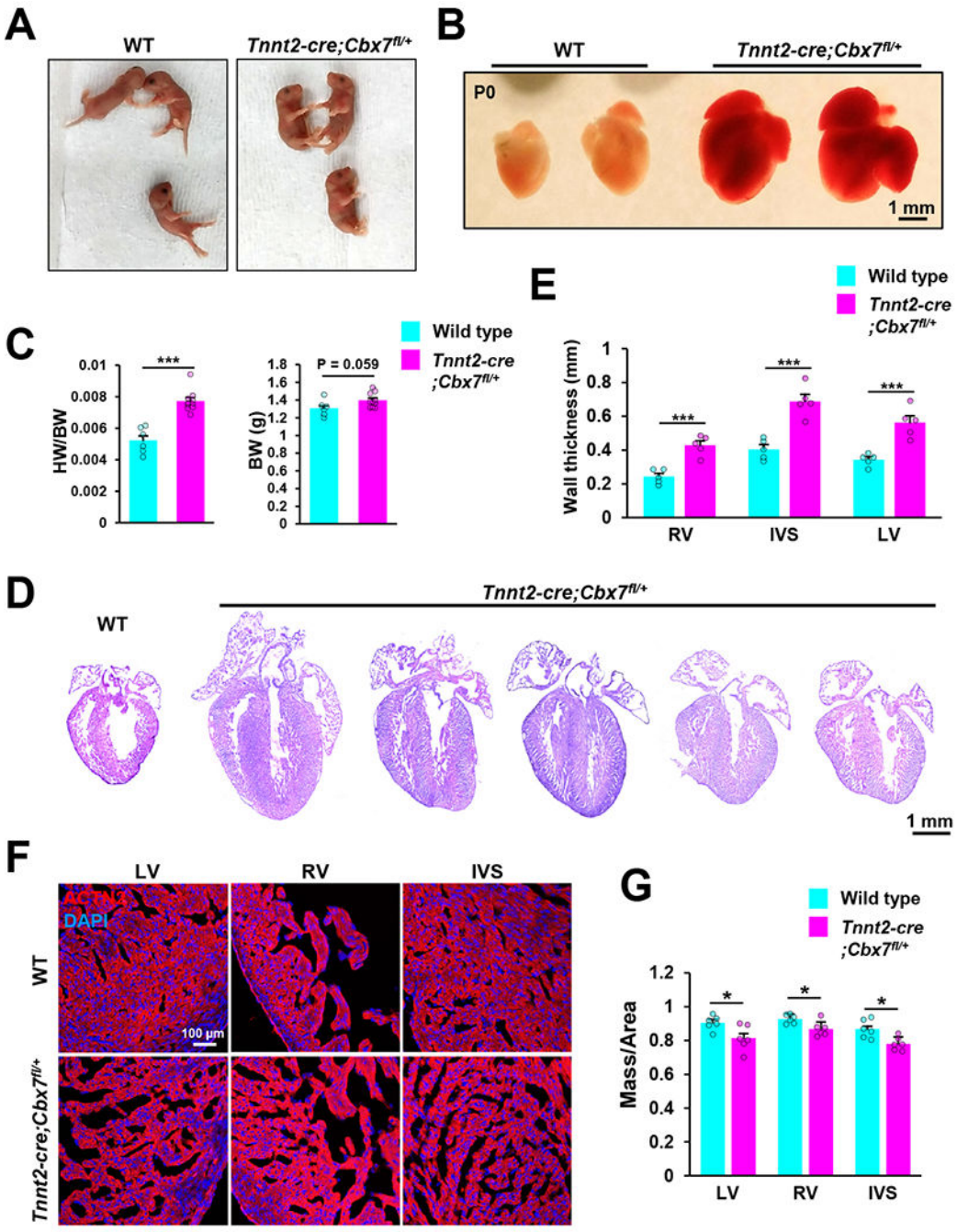

Figure 2. Neonatal lethality, cardiomegaly, thickening of ventricular walls, and impeded myocardial compaction by cardiomyocyte-specific inhibition of CBX7.

A. Representative photographs of neonatal (P0) wild-type and *Tnnt2-Cre;Cbx7*$^{fl/+}$ mice. **B.** Representative pictures of neonatal (P0) mouse hearts from wild-type and *Tnnt2-Cre;Cbx7*$^{fl/+}$ mice. **C.** The heart to body weight ratio (left) and the body weight (right). ***P < 0.001. Standard unpaired Student's t test. N = 6 for the wild-type and N = 10 for the mutant, each with technical triplicates. **D.** H&E stained images of the wild-type and *Tnnt2-Cre;Cbx7*$^{fl/+}$ hearts in a four chamber view. **E.** Wall thickness of RV, IVS, and

LV in wild-type and *Tnnt2-Cre;Cbx7*$^{fl/+}$. *P < 0.05, **P < 0.01, ***P < 0.001. Standard unpaired Student's t test. N = 5, each with technical triplicates. **F.** Representative confocal microscopic images of the LV, RV, and IVS of control (upper panel) and *Tnnt2-Cre;Cbx7*$^{fl/+}$ (lower panel) mice at P0 stained for ACTN2 and DAPI. **G.** Quantification of mass per area. *P < 0.05, **P < 0.01, ***P < 0.001. Standard unpaired Student's t test. N = 6, each with technical triplicates.

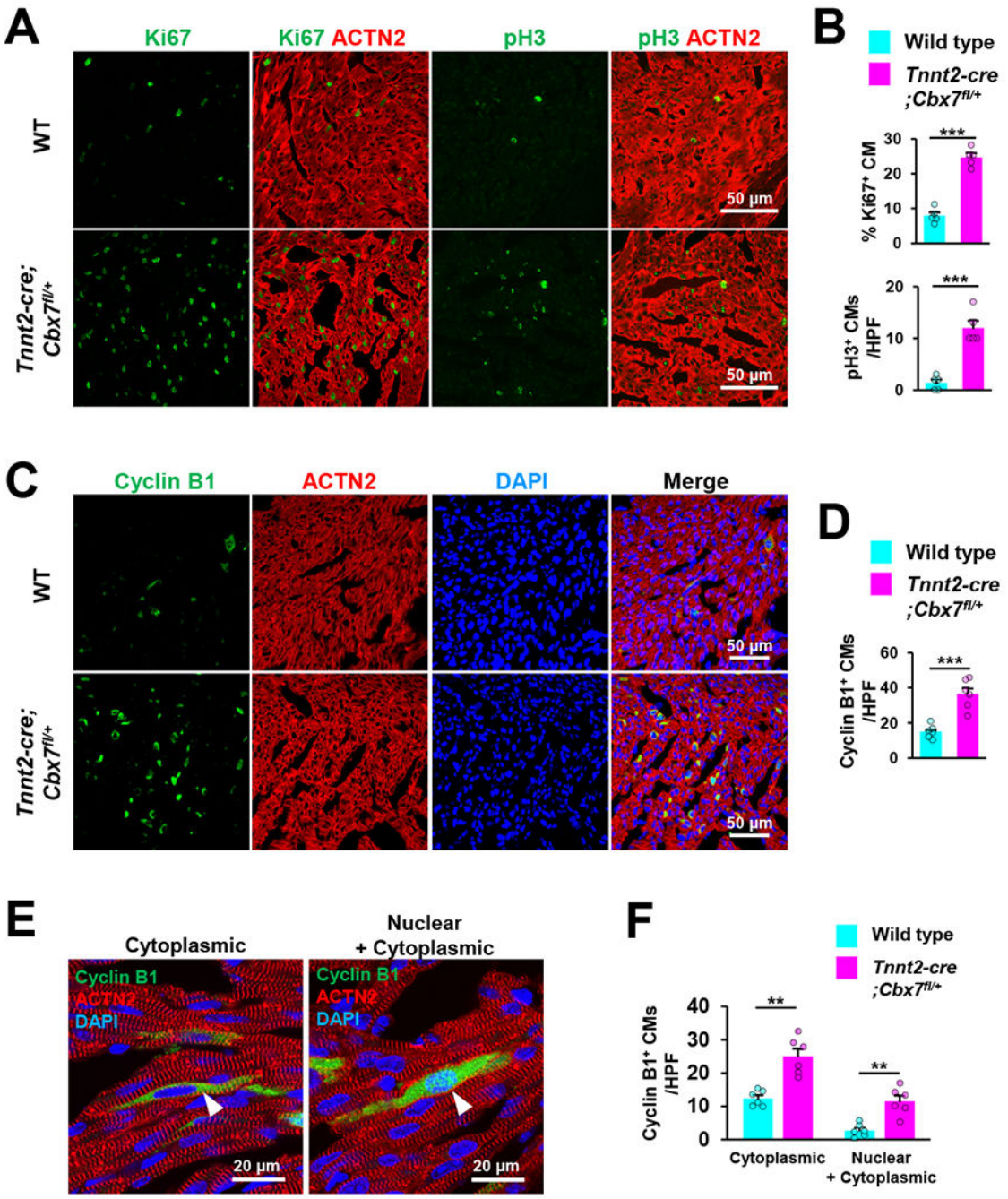

Figure 3. Increased CM proliferation in the neonatal heart by targeted inhibition of CBX7.

A. Representative confocal microscopic images of neonatal (P0) hearts from wild-type and *Tnnt2-Cre;Cbx7*$^{fl/+}$ mice stained for ACTN2, Ki67, and pH3. **B.** Quantification of Ki67^{+} or pH3^{+} CMs out of total CMs. ***P < 0.001. Standard unpaired Student's t test. N = 5. More than 5000 cells in each group were examined. HPF, High-power field (X10). **C-F.** Results from immunostaining of neonatal (P0) hearts from wild-type and *Tnnt2-Cre;Cbx7*$^{fl/+}$ mice with cyclin B1 and ACTN2. DAPI (blue). Representative confocal microscopic images stained for cyclin B1 and ACTN2 at low magnification (**C**) and their quantification (**D).**

***P < 0.001, Standard unpaired Student's t test. N = 6. More than 5000 cells in each group were examined. Representative confocal microscopic images showing two different subcellular localizations of cyclin B1 in CMs (**E**) and their quantification (**F**). **P < 0.01, ***P < 0.001. Standard unpaired Student's t test. N = 6. 300 cyclin $B1^+$ CMs in 5 different fields were examined.

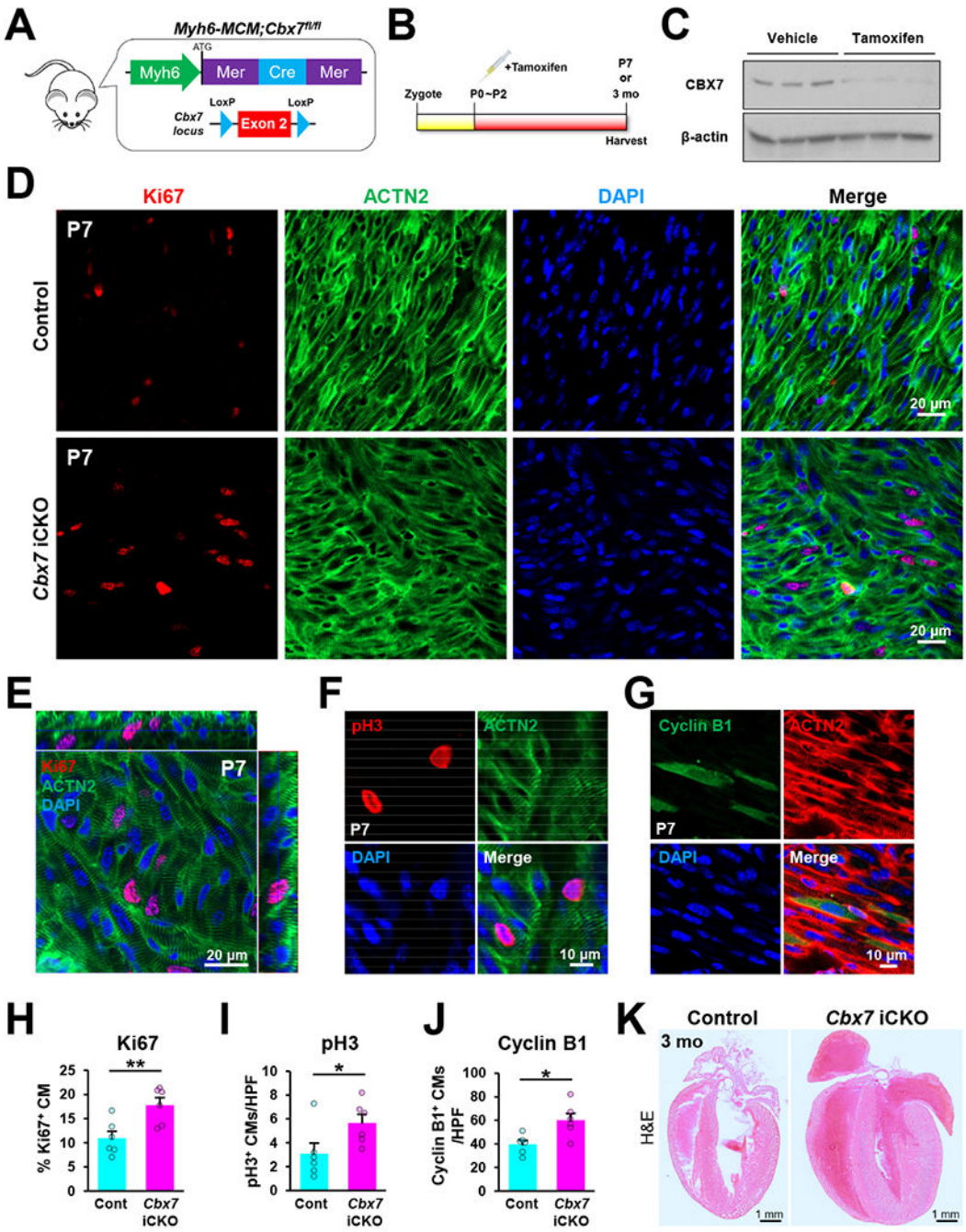

Figure 4. Increased CM proliferation in the postnatal heart by targeted inhibition of CBX7.

A. A schematic showing the genotype of inducible conditional knockout mice (*Myh6-MCM;Cbx7*$^{fl/fl}$). Exon 2 of *Cbx7* gene is genetically deleted in CMs upon tamoxifen treatment. **B.** The experimental timeline for postnatal deletion of *Cbx7* in CMs. Vehicle (Control) or tamoxifen (*Cbx7* iCKO) were subcutaneously administered to neonatal mice at P0-P2 and the hearts were harvested at P7 or 3 months (mo). **C.** Validation of CBX7 deletion via western blotting with hearts collected from *Myh6-MCM;Cbx7*$^{fl/fl}$ mice at 3 mo. N = 3, each with technical triplicates. **D.** Representative confocal microscopic images

of P7 hearts from *Myh6-MCM;Cbx7*$^{fl/fl}$ mice immunostained for Ki67, ACTN2. DAPI (blue). **E.** A representative orthogonal projection image of tamoxifen-treated P7 hearts from *Myh6-MCM;Cbx7*$^{fl/fl}$ mice in panel D. **F.** Representative confocal microscopic images of P7 hearts from *Myh6-MCM;Cbx7*$^{fl/fl}$ mice (tamoxifen treated) immunostained for pH3, ACTN2. DAPI (blue). **G.** Representative confocal microscopic images of P7 hearts from *Myh6-MCM;Cbx7*$^{fl/fl}$ mice immunostained for cyclin B1, ACTN2. DAPI (blue). **H-J.** Quantification of CMs positive for Ki67 (H), pH3 (I), and cyclin B1 (J) in P7 hearts from *Myh6-MCM;Cbx7*$^{fl/fl}$ mice. *P < 0.05, **P < 0.01. Standard unpaired Student's t test. N = 6. More than 5000 cells in each group were examined. **K.** Representative H & E stained images of 3-month-old hearts from *Myh6-MCM;Cbx7*$^{fl/fl}$ mice.

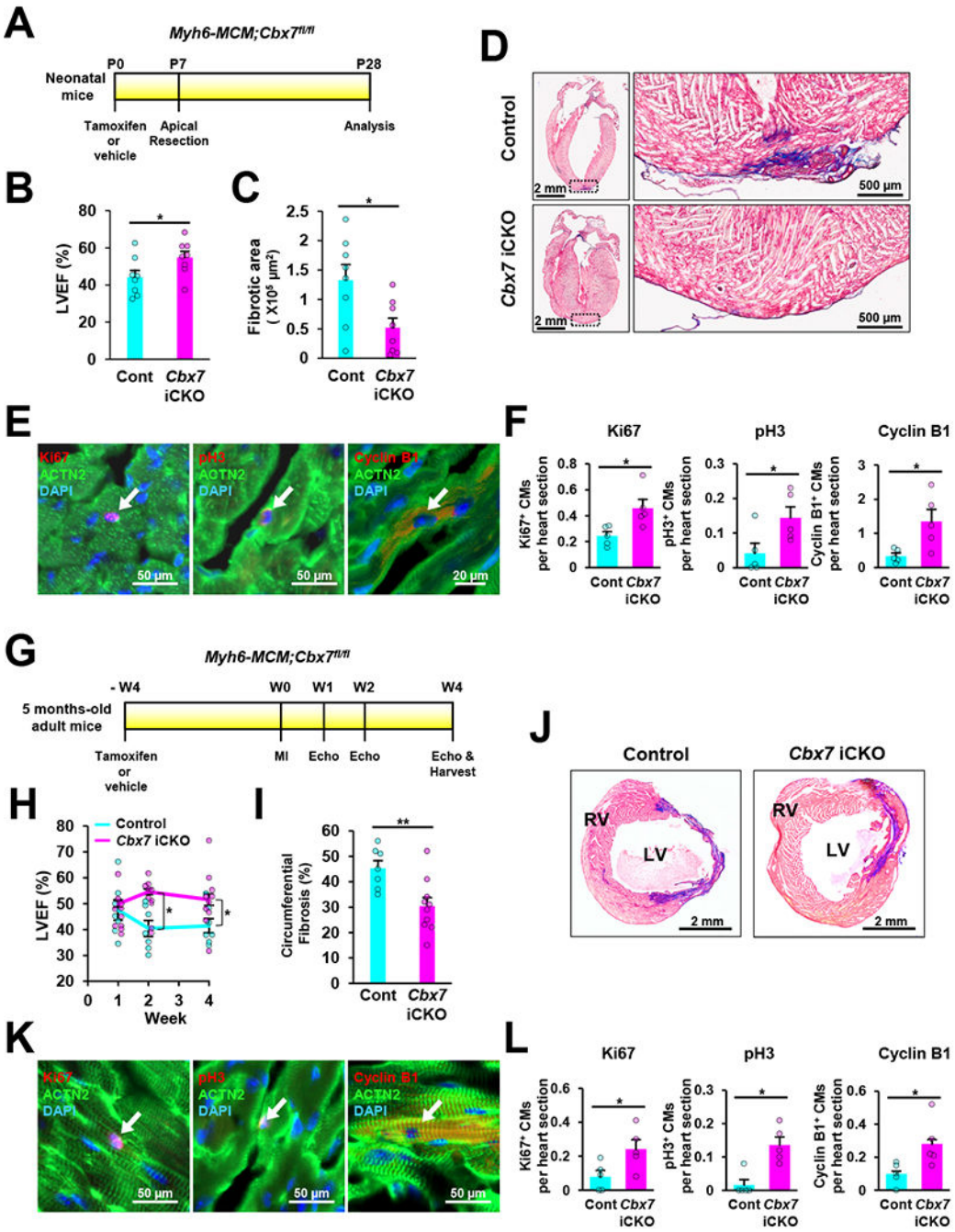

Figure 5. Augmented regeneration of neonatal and adult hearts by targeted inhibition of CBX7.

A. The experimental timeline for cardiac apical resection model. Vehicle (Control) or tamoxifen (*Cbx7* iCKO) were administered to neonatal mice at P0, which underwent cardiac apical resection surgery at P7, and the hearts were harvested at P28. **B.** Echocardiographic analyses at P28. LVEF, left ventricular ejection fraction. *P < 0.05. Standard unpaired Student's t test. N = 8. **C.** Quantitative analyses of fibrosis area at P28. *P < 0.05. Standard unpaired Student's t test. Standard unpaired Student's t test. N = 8. **D.** Representative 4-chamber view images of Masson's trichrome-stained hearts at P28. Apex was enlarged

on the right. **E.** Representative confocal microscopic images of P28 hearts from *Myh6-MCM;Cbx7*$^{fl/fl}$ mice (tamoxifen treated) immunostained for Ki67, pH3, cyclin B1, and ACTN2. DAPI (blue). Arrows indicate CMs positive for either Ki67, pH3, or cyclin B1. **F.** Quantification of CMs positive for Ki67, pH3, and cyclin B1 in P7 hearts from *Myh6-MCM;Cbx7*$^{fl/fl}$ mice. *P < 0.05. Standard unpaired Student's t test. N = 5. **G.** The experimental timeline for the myocardial infarction (MI) model. Vehicle (Control) or tamoxifen (*Cbx7* iCKO) were administered to adult mice (5-months-old). Four weeks later, mice underwent MI surgery. Echocardiographic analyses were performed at W1, W2, and W4. Hearts were harvested at W4 for histological analyses. **H.** Echocardiographic analyses at W1, W2, and W4. *P < 0.05. Standard unpaired Student's t test. N = 7-10. **I.** Quantitative analyses of fibrosis area at W4. **P < 0.01. Standard unpaired Student's t test. N = 7-10. **J.** Representative cross-sectional images of Masson's trichrome-stained hearts at W4. **K.** Representative confocal microscopic images of W4 hearts from *Myh6-MCM;Cbx7*$^{fl/fl}$ mice (tamoxifen treated) immunostained for Ki67, pH3, cyclin B1, and ACTN2. DAPI (blue). Arrows indicate CMs positive for either Ki67, pH3, or cyclin B1. **L.** Quantification of CMs positive for Ki67, pH3, and cyclin B1 in W4 hearts from *Myh6-MCM;Cbx7*$^{fl/fl}$ mice. *P < 0.05. Standard unpaired Student's t test. N = 5.

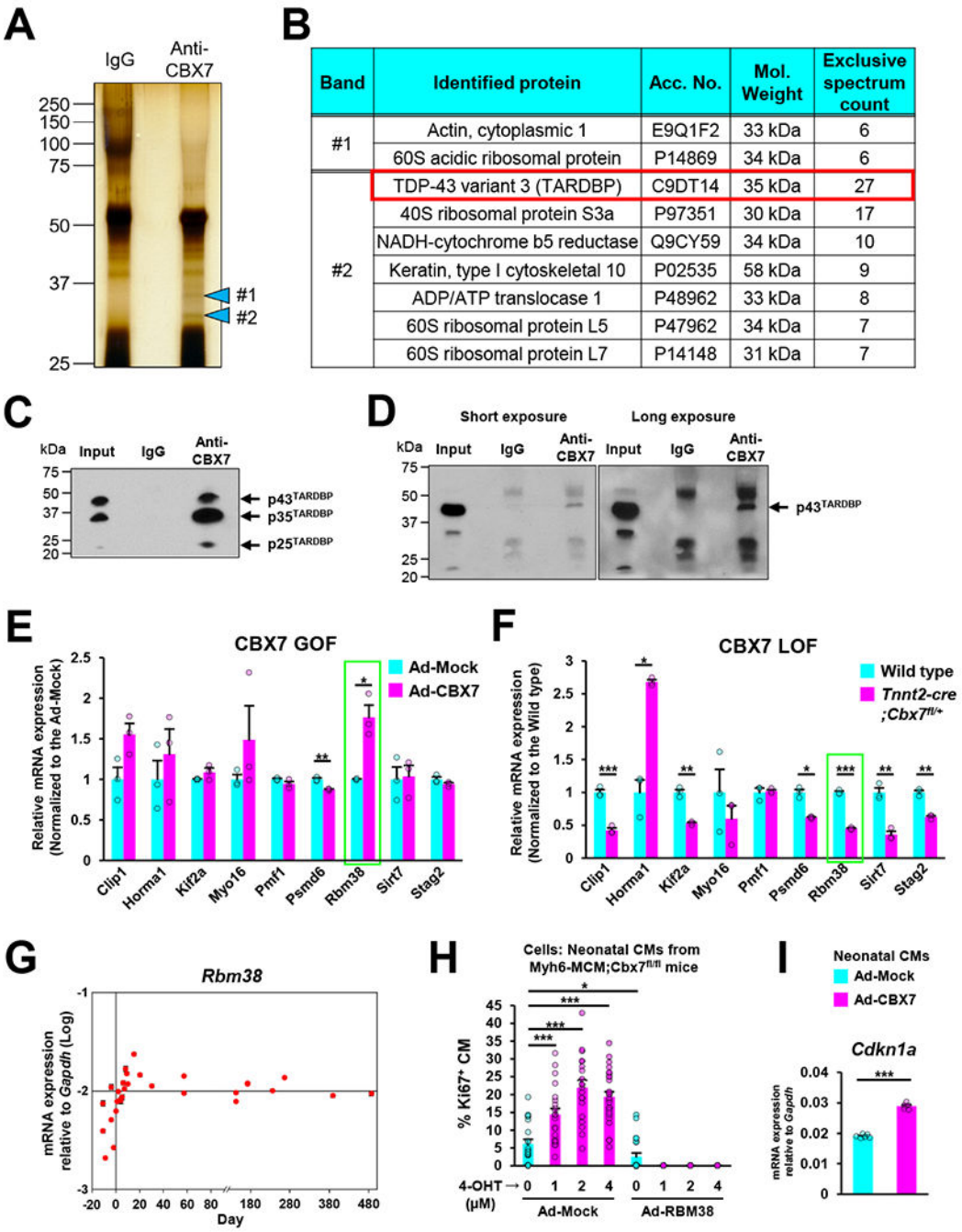

Band	Identified protein	Acc. No.	Mol. Weight	Exclusive spectrum count
#1	Actin, cytoplasmic 1	E9Q1F2	33 kDa	6
	60S acidic ribosomal protein	P14869	34 kDa	6
#2	TDP-43 variant 3 (TARDBP)	C9DT14	35 kDa	27
	40S ribosomal protein S3a	P97351	30 kDa	17
	NADH-cytochrome b5 reductase	Q9CY59	34 kDa	10
	Keratin, type I cytoskeletal 10	P02535	58 kDa	9
	ADP/ATP translocase 1	P48962	33 kDa	8
	60S ribosomal protein L5	P47962	34 kDa	7
	60S ribosomal protein L7	P14148	31 kDa	7

Figure 6. Interaction of CBX7 and TARDBP and its impact on expression of mitosis-related genes.

A. Immunoprecipitation of CBX7 binding partners. Mouse CBX7 was overexpressed in mouse embryonic fibroblasts (MEFs) via Ad-CBX7. The cytoplasmic protein fraction was isolated and immunoprecipitated using either IgG (control) or anti-CBX7 antibody. Immunoprecipitated samples were subjected to SDS-PAGE followed by silver staining. Indicated bands (#1 and #2) represent candidates for CBX7 binding partners. **B**. Identified peptides for CBX7 binding partners. Band slices for #1 and #2 underwent MALDI-

TOF followed by mass spectrometry. Identified proteins with more than 6 exclusive spectrum counts were listed. Probability for all the listed proteins is higher than 95%. **C-D**. Immunoprecipitation for TARDBP. The cytoplasmic protein fraction was isolated from MEFs treated with Ad-CBX7 (C) or 3-month-old adult mouse hearts (D) and was immunoprecipitated using either IgG (control) or anti-CBX7 antibody. Immunoprecipitated samples were subjected to SDS-PAGE followed by western blotting with an anti-TARDBP antibody. Input was used as a positive control. Three independent experiments, each with technical triplicates. **E**. mRNA expression of TARDBP target genes in CBX7-overexpressing CMs. Neonatal mouse CMs were treated with Ad-Mock or Ad-CBX7 for three days and underwent qRT-PCR. Gene expression levels were normalized to *Gapdh*. *P < 0.05, ***P < 0.001. Standard unpaired Student's t test. Three independent experiments, each with technical triplicates. GOF: gain of function. **F**. mRNA expression of TARDBP target genes in *Cbx7*-haplodeficient (*Tnnt2-Cre;Cbx7*$^{fl/+}$) mouse hearts in comparison with neonatal (P0) hearts. Gene expression measured by qRT-PCR and normalized to *Gapdh*. *P < 0.05, **P < 0.01, ***P < 0.001. Standard unpaired Student's t test. Three independent experiments, each with technical triplicates. LOF: loss of function **G**. mRNA expression of *Rbm38* gene in the mouse hearts from E10.5 to 486 days after birth. qRT-PCR results. N = 31, each with technical triplicates. **H**. Percentages of Ki67^{+} CMs upon *Cbx7* knockout and *Rbm38* overexpression. CMs were isolated from neonatal (P1) *Myh6-MCM;Cbx7*$^{fl/fl}$ mice and treated with Ad-Mock or Ad-RBM38 in the presence of 4-OHT at different concentrations. Cells were cultured for 5 days in the absence of growth factors including IGF-1 and FGF-1. *P < 0.05, ***P < 0.001. One-way ANOVA test with Tukey HSD. Three independent experiments. More than 500 cells in each group were examined. **I**. mRNA expression of *Cdkn1a* gene in neonatal CMs treated with Ad-Mock or Ad-CBX7. Neonatal (P0) mouse CMs were treated with adenoviral particles for 3 days and subjected to qRT-PCR. ***P < 0.001. Standard unpaired Student's t test. The representative data for three independent experiments, each with six technical replicates.